DEPOSITION AND CHARACTERIZATION OF MESOPOROUS SILICA COATINGS ON MAGNESIUM ALLOYS

by

Afrah Al Hegy

A thesis submitted in partial fulfillment
of the requirements for the degree of
Master of Science (MSc) in Chemical Sciences

The School of Graduate Studies
Laurentian University
Sudbury, Ontario, Canada

© Afrah Al Hegy, 2014

THESIS DEFENCE COMMITTEE/COMITÉ DE SOUTENANCE DE THÈSE

Laurentian Université/Université Laurentienne
School of Graduate Studies/École des études supérieures

Title of Thesis Titre de la thèse	DEPOSITION AND CHARACTERIZATION OF MESOPOROUS SILICA COATINGS ON MAGNESIUM ALLOYS
Name of Candidate Nom du candidat	Al Hegy, Afrah
Degree Diplôme	Master of Science

Department/Program Département/Programme	Chemical Sciences	Date of Defence Date de la soutenance	February 07, 2014

APPROVED/APPROUVÉ

Thesis Examiners/Examinateurs de thèse:

Dr. Joy Gray-Munro
(Supervisor/Directrice de thèse)

Dr. Nelson Belzile
(Committee member/Membre du comité)

Dr. Louis Mercier
(Committee member/Membre du comité)

Dr. Marta G. Cerruti
(External Examiner/Examinatrice externe)

Approved for the School of Graduate Studies
Approuvé pour l'École des études supérieures
Dr. David Lesbarrères
M. David Lesbarrères
Director, School of Graduate Studies
Directeur, École des études supérieures

ACCESSIBILITY CLAUSE AND PERMISSION TO USE

I, **Afrah Al Hegy**, hereby grant to Laurentian University and/or its agents the non-exclusive license to archive and make accessible my thesis, dissertation, or project report in whole or in part in all forms of media, now or for the duration of my copyright ownership. I retain all other ownership rights to the copyright of the thesis, dissertation or project report. I also reserve the right to use in future works (such as articles or books) all or part of this thesis, dissertation, or project report. I further agree that permission for copying of this thesis in any manner, in whole or in part, for scholarly purposes may be granted by the professor or professors who supervised my thesis work or, in their absence, by the Head of the Department in which my thesis work was done. It is understood that any copying or publication or use of this thesis or parts thereof for financial gain shall not be allowed without my written permission. It is also understood that this copy is being made available in this form by the authority of the copyright owner solely for the purpose of private study and research and may not be copied or reproduced except as permitted by the copyright laws without written authority from the copyright owner.

Abstract

In recent years, magnesium and magnesium alloys have received much attention as a new biomaterial in orthopaedic applications due to their biodegradability, biocompatibility, and their mechanical properties that are similar to natural bone tissue. The most common problem associated with magnesium as a biomaterial is low corrosion resistance in physiological solutions. This decreases the mechanical integrity of the implants in the early stages of healing and has a negative impact on the overall biocompatibility. The main goal of this study was to create a multi-layered coating consisting of a silica sol-gel under-layer to protect the substrate from corrosion in body fluids and a mesoporous silica top-layer to enhance the bioactivity of the coated implant material.

The results indicate that the deposited multi-layered coating enhances both the bioactivity and the corrosion resistance of the material.

Keywords

Biomaterials, biodegradable, orthopaedic implants, magnesium alloys, corrosion resistance, bioactivity, silane coating, mesoporous silica coating

Acknowledgments

I would like to express my appreciation to Dr. Joy Gray-Munro for giving me the opportunity to study in her lab. I would also like to think her for her support throughout my thesis as well as her patience, knowledge, and advice which allowed me to develop an understanding of this study.

I would like to extend my thanks to my committee members Dr. L. Mercier and Dr. N. Belzile for their time, support throughout my study and for reviewing my thesis.

I would also like to thank all of my lab mates, past and present, especially Xiaoxi Yang, Sahejmeet Guraya and Thomas Bizley.

I would also like to share the accomplishment of this thesis with my Mother Salama Shibib for her encouragement and patience when it was most needed and my lovely husband Habib Alkhames for his support and for standing by my side throughout this entire journey.

I would also like to thank my family and friends for their continuous encouragement.

Finally, I would like to acknowledge the financial support provided by the Ministry of Higher Education in the Kingdom of Saudi Arabia.

Table of Contents

Thesis Defence Committee ..... **Error! Bookmark not defined.**

Abstract iii

Acknowledgments iv

Table of Contents v

List of Tables vii

List of Figures viii

1 List of Reaction Schemes x

List of Abbreviations xi

Chapter 1 1

1 « Introduction » 1

1.1 Magnesium and its Alloys as Orthopaedic Biomaterials 2

1.1.1 Biocompatibility of Magnesium 2

1.1.2 Biodegradability of Magnesium 2

1.1.3 Mechanical Properties of Magnesium 4

1.2 Limitations of Using Magnesium as a Biomaterial 6

1.2.1 Magnesium Corrosion Resistance 6

1.2.2 Corrosion Prevention 8

1.3 Protective and Bioactive Coatings on Magnesium Alloy AZ31 9

1.3.1 Silane as a Protective Coating 9

1.3.2 Mesoporous Silica as a Bioactive Coating 13

1.4 Objectives of the Thesis 20

Chapter 2 22

2 « Materials and Methods » 22

2.1 Materials 22

2.2 Methods 24
2.2.1 Polishing AZ31 Mg Alloy 26
2.2.2 Cleaning 26
2.2.3 Alkaline Aging 26
2.2.4 Coating Procedures 26
2.2.5 Corrosion Test 28
2.2.6 Bioactivity Test 28
2.2.7 Instrumental Analysis 29
Chapter 3 33
3 « Results and Discussion » 33
3.1 Optimization of Sol-gel Silica Pre-layer Coating Conditions 33
3.1.1 Control Sample of Magnesium Alloy AZ31 34
3.1.2 Study on the Influence of TEOS Concentration 36
3.1.3 Study on the Influence of Deposition Time of TEOS 37
3.1.4 Study on the Influence of the Deposition Time and TEOS Concentration on Thickness and Uniformity of the Sol-gel Silica Coating 38
3.2 Deposition of Mesoporous Silica as a Bioactive Coating 39
3.2.1 Optimization of Mesoporous Silica Coating Conditions on Bare Magnesium Alloy AZ31 39
3.3 Characterization of the Multi-layered, Bi-Functional Coating (Sol-gel Silica Coating + Mesoporous Silica Film) 49
3.4 Corrosion Test (FAAS) 52
3.5 Study on the Bioactivity of the Multi-layered Film: 54
Chapter 4 62
4 « Conclusions and Future Direction » 62
5 References 63

List of Tables

Table 1-1: Summary of the Physical and Mechanical Properties of Various Implant Materials in Comparison to Natural Bone 5

Table 2-1: The Composition (% mass) of Magnesium Alloy AZ31. 22

Table 2-2: Table of Chemicals. 23

Table 2-3: The Composition of Hanks Balanced Salt Solution. 23

Table 2-4: Sol-Gel Silica Coating Solution Composition 27

Table 3-1: The Atomic Percentages of Mg-Si-P-Ca after Immersion the Coated and Uncoated (Control) Samples in SBF for Different Times 61

List of Figures

Figure 1-1: Pourbaix Diagram for Magnesium 4

Figure 1-2: The Molecular Structure of Tetraethoxysilane (TEOS). 10

Figure 1-3: Surfactant in Aqueous Solution. 15

Figure 1-4: The Molecular Structure of Dodecyltrimethylammonium Chloride (DTAC) 15

Figure 1-5: The Synthesis Mechanism of Mesoporous Silica Materials 16

Figure 2-1: An Overview of the Experimental Procedure. 25

Figure 2-2: IUPAC Isotherms Types and Types of Hysteresis Loops 31

Figure 3-1: IR Spectrum of Mg alloy AZ31 after Surface Pretreatment. 34

Figure 3-2: IR Spectrum for TEOS. 35

Figure 3-3: IR Spectra for Sol-gel Silica Coating on Magnesium Alloy AZ31 at Various Concentrations of TEOS. 36

Figure 3-4: IR Spectra for Mg Alloy AZ31 Coated with 3.2% TEOS at Various Deposition Times 37

Figure 3-5: Graph of Silica Peak Areas as a Function of Deposition Time and Concentration of TEOS 38

Figure 3-6: IR Spectrum for Surfactant on Mg Alloy AZ31 40

Figure 3-7: IR Spectrum for Particles Layers on Mg Alloy AZ31 41

Figure 3-8: IR Spectra of As-Deposited Mesoporous Silica Films at Various Deposition Times 42

Figure 3-9: IR Spectra for Multiple Mesoporous Silica Treatments 43

Figure 3-10: IR Spectra for Multiple Mesoporous Silica Treatments 44

Figure 3-11: IR Spectra for Three Different Spots on an As-Deposited Mesoporous Silica coating as a function of successive treatments/dips in the coating bath. (Deposition time for each layer was 20 min.) 45

Figure 3-12: 5 µm x 5 µm TM-AFM Images for Magnesium Alloys Coated with as Deposited Mesoporous Silica as a Function Number of Treatments/Layers 46

Figure 3-13: IR Spectra for Magnesium Alloys Coated with Multiple Treatments of Mesoporous Silica after and before Calcination 48

Figure 3-14: IR Spectra for Magnesium Alloys Coated with Multiple Treatments of Mesoporous Silica after and before Calcination 48

Figure 3-15: IR Spectra for the Final Multi-layered Coating (Sol-gel Silica Coating + Mesoporous Silica Film) before and after Calcination 50

Figure 3-16: N_2 Adsorption/Desorption Isotherms of the Mesoporous Silica Coating 51

Figure 3-17: Amount of Magnesium Dissolved as a Function of Immersion Time in SBF 53

Figure 3-18: SEM Images of Coated and Uncoated Mg AZ31 Alloys after Immersion in SBF for Different of Time; (a) Uncoated (b) Coated Sample after 1 Day Immersion, (c) Uncoated (d) Coated after 3 Days Immersion, (e) Uncoated (f) Coated after 7 Days Immersion 56

Figure 3-19: The Ratio of Ca/Mg after Immersion the Coated and Uncoated (Control) Samples in SBF for Different Times 58

Figure 3-20: The Ratio of Silicon/Magnesium after Immersion the Coated Samples in SBF for Different Times 59

Figure 3-21: IR Spectra for the Final Multi-layered Coating after Immersion in SBF for Various Periods of Time 60

1 List of Reaction Schemes

Reaction Scheme 1.1: General Corrosion Mechanism of Magnesium. 7

Reaction Scheme 1.2: Influence of Anions. 7

Reaction Scheme 1.3: Precipitation Reactions. 8

Reaction Scheme 1.4: Silane Chemistry. 11

Reaction Scheme 3.1: Precipitation Reactions. 55

List of Abbreviations

AFM	- Atomic Force Microscope
ATR-FTIR	- Attenuated Total Reflectance-Fourier Transform Infrared Spectroscopy
Mg AZ31	- Magnesium Alloy containing 96 % Magnesium, 3% Aluminum, 1% Zinc
SBF	- Simulated Body Fluid
FAA	- Flame Atomic Absorption
SEM-EDS	- Scanning Electron Microscopy-Energy Dispersive Spectroscopy
MCM	- Mobile Crystalline Materials
SBA	- Santa Barbara Amorphous
MSU	- Michigan State University
FDU	- FuDan University
KIT	- Korea Advanced Institute of Science and Technology
IUPAC	- International Union of Pure and Applied Chemistry

Chapter 1

1 « Introduction »

Synthetic materials have been used extensively in medical applications. Materials used for these applications are known as biomaterials. The term biomaterial has been defined by the European Society for Biomaterials Consensus Conference as “A material intended to interface with biological systems to evaluate, treat, augment or replace any tissue, organ, or function of the body” [1].

Biomaterials are used in the replacement and treatment of diseased or injured tissue in different parts of the body; some examples include cardiovascular, dental and orthopaedic implants [3]. The development of biomaterials for orthopaedic applications has been a significant challenge to biomaterials scientists. The optimum biomaterials for orthopaedic implants should be non-toxic and biocompatible with the human body [2]. Furthermore, they should have excellent mechanical properties for the intended application and under some circumstances these biomaterials should be biodegradable to prevent the need for additional surgery to remove the implant after healing has occurred [4].

Biomaterials can be classified according to their structural, chemical, and biological properties. Orthopaedic biomaterials are classified as bioinert, bioactive or bidegradable depending on how they interface with the body tissue [5]. The term bioinert refers to any materials such as stainless steel, alumina and titanium which are designed to have minimal interaction with the surrounding tissue when they are placed in the human body. On the other hand, bioactive biomaterials such as synthetic hydroxyapatite, glass-ceramic A-W and bioglass® are designed to specifically interact with the surrounding tissue during implantation resulting in the formation of a hydroxyapatite layer on the implant surface that enhances the biocompatibility of the material. Finally, biodegradable biomaterials such as tricalcium phosphate, synthetic polymers and magnesium are materials that are designed to dissolve or degrade after the tissue has healed [6]. However, these biodegradable biomaterials need to maintain their mechanical properties

until the implant is no longer needed and then they must be absorbed and eliminated from the body as non-toxic degradation products [7].

1.1 Magnesium and its Alloys as Orthopaedic Biomaterials

Magnesium alloys have the highest strength/weight ratio of all known structural metals. They are a third lighter than aluminum and a quarter the density of steel [8]. In recent years, magnesium and its alloys have received much attention as potential orthopaedic biomaterials due to their excellent biocompatibility, biodegradability, and mechanical properties that are similar to natural bone. These properties have made magnesium alloys a promising alternative for biodegradable orthopaedic implants that decrease stress shielding and enhance new bone growth [8-9].

1.1.1 Biocompatibility of Magnesium

Magnesium is the fourth most abundant inorganic element in the human body. The average adult human body weighs around 70 kg and contains from 21 – 28 g of magnesium [10-11]; 50 percent of this total body magnesium is stored in the skeletal system. To maintain appropriate magnesium levels in the body, humans need to absorb between 300 to 400 mg of magnesium daily [11]. Moreover, magnesium is also essential to human metabolic functions such as DNA/RNA stabilization and it acts as a co-factor for more than 300 different enzymatic reactions. It has also been shown to promote bone cell attachment and tissue growth on implant materials [8-12]. Magnesium influences many biological functions within the body and plays a very important role within the cell [13-14], therefore, it can be concluded that magnesium is non-toxic.

1.1.2 Biodegradability of Magnesium

Metallic materials such as stainless steel, cobalt-based alloys and titanium alloys are widely used as biomaterials due to their flexibility, high strength and excellent corrosion resistance. However, these implants are not biodegradable in the human body. Toxic ions can be released when these implants corrode, which results in inflammation and tissue loss [15]. Furthermore, in some cases, such as fracture fixation, these metallic implants

are only needed for a short time until the healing process has occurred. This means that a second surgery may be necessary to remove the implant after tissue healing [15-16]. Biodegradable metallic materials that can provide the required stability during the initial stages of healing and promote tissue regeneration as they degrade would eliminate both the toxic corrosion products associated with traditional metallic implants and the need for a second surgery. The anodic dissolution of magnesium results in the release of non-toxic magnesium ions that can easily be excreted in the urine [17]. In other words, magnesium implants can gradually be dissolved, absorbed and excreted after the healing process. Therefore, patients would not need a second surgery operation to remove the implant [18]. Unfortunately, the rate of magnesium degradation is normally too fast in the initial stage after implantation. Therefore, it is important to control the surface degradation of biomaterials after implantation into the human body because tissue healing takes time [19]. This is illustrated in the Pourbaix diagram of magnesium (Figure 1.1) which shows that magnesium has good corrosion resistance in alkaline solution due to the formation of a passive $Mg(OH)_2$ film on the surface that is stable in solution of pH > 12. In contrast, studies have shown that magnesium is highly degradable in both acidic solution and at the neutral pH conditions typically observed in the physiological environment [20].

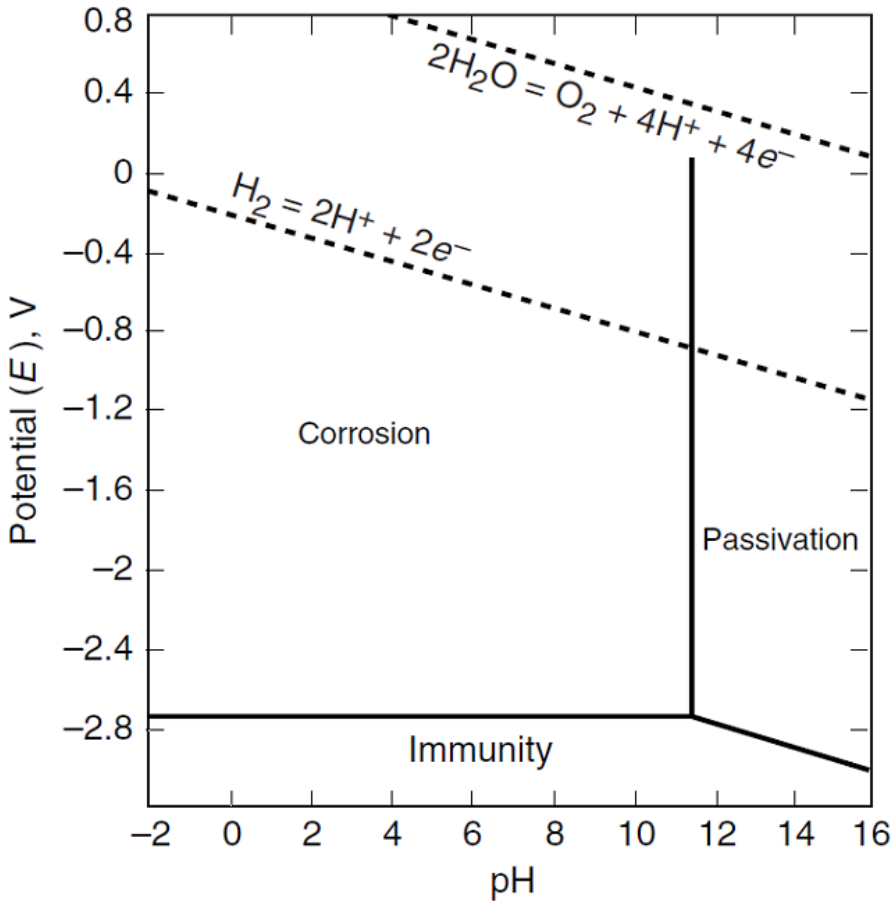

Figure 1-1: Pourbaix Diagram for Magnesium. [20]

1.1.3 Mechanical Properties of Magnesium

There are four major types of biomaterials: metals, polymers, ceramics and glasses [21]. Some metals play an important role as biomaterials to assist with the repair of bone tissue that has been damaged or diseased [8]. Metallic materials are more suitable for load-bearing applications compared with polymeric or ceramics materials due to their high mechanical strength and fracture toughness [19]. Commonly implanted metallic biomaterials include stainless steels, titanium and cobalt–chromium-based alloys [19]. One of the main drawbacks in using these is their difference in mechanical and physical properties in comparison to natural bone tissue which might result in implant failure due to the stress shielding effect [8-21]. The stress shielding effect is the reduction in the

density of bone tissue due to the removal of the normal stress on the bone after implantation. The bone in a healthy person will remodel in response to an applied load. Therefore, the bone will become weaker if the loading on bone decreases due to the difference in the stiffness between natural bone tissue and the implant material [22].

In contrast, magnesium has physical and mechanical properties that are more similar to natural bone than traditional metallic implant materials. A brief summary is given in Table 1.1 which shows that the density of pure magnesium is approximately 1.74 g/cm^3, it is 1.6 times less dense than aluminum and 4.5 times less dense than steel making it the structural metal with a density closest to that of human bone tissue (1.8 g/cm^3). Furthermore, the fracture toughness of magnesium is greater than of ceramic biomaterials such as hydroxyapatite. The elastic modulus and compressive yield strength of magnesium are also the same order of magnitude as that of natural bone (Table 1.1) [8]. These similarities to natural bone should help in reducing or avoiding the stress shielding effect thus enhancing stimulation and remodeling of the bone tissue.

Table 1-1: Summary of the Physical and Mechanical Properties of Various Implant Materials in Comparison to Natural Bone [8].

Properties	Natural bone	Pure Magnesium	Ti alloy	Co–Cr alloy	Stainless steel	Synthetic hydroxyapatite
Density (g/cm^3)	1.8–2.1	1.74–2.0	4.4–4.5	8.3–9.2	7.9–8.1	3.1
Elastic modulus (GPa)	3–20	41–45	110–117	230	189–205	73–117
Compressive yield strength (MPa)	130–180	65–100	758–1117	450–1000	170–310	600
Fracture toughness (MPa/m$^{1/2}$)	3–6	15–40	55–115	N/A	50–200	0.7

1.2 Limitations of Using Magnesium as a Biomaterial

Application of magnesium as an implant material has been limited due to its high corrosion rate in the body fluid and its rapid degradation before the surrounding tissue has sufficiently healed [23]. The high degradation rate not only influences tissue healing but can also cause the loss of the mechanical integrity of the implant itself before the bone tissue has healed sufficiently to be able to bear weight. This can lead to the occurrence of a second fracture [24]. Orthopaedic biomaterials require around three to four months for bone regeneration. To avoid a second fracture, magnesium alloy implants should maintain their mechanical properties for at least three months while the bone tissue heals [24].

1.2.1 Magnesium Corrosion Resistance

As stated previously, poor corrosion resistance is the major problem that has limited the widespread use of magnesium alloys. The chemical and electrochemical reactivity of magnesium alloys are considered high when compared with other structural metals such as steels and aluminum alloys. There are two key factors that lead to poor corrosion resistance for magnesium alloys. The first is internal galvanic corrosion due to the presence of secondary phases or impurities. For magnesium aluminum alloys, the β phase consists of second phase particles that precipitate at the grain boundaries during solidification. These β phase particles have the stoichiometric composition, Mg_{17} Al_{12}, therefore they are aluminum rich in comparison to the magnesium rich, α phase, of the material. Due to the difference in electrochemical potential between the metals, internal galvanic coupling can occur resulting in increased corrosion rates [25-26]. The second factor leading to poor corrosion resistance is the limited stability of the hydroxide film that forms on magnesium surfaces. These hydroxide films are typically less stable than passive films that form on other materials such as aluminum alloys and stainless steel [27].

1.2.1.1 Corrosion Mechanism of Magnesium in SBF

The corrosion reaction of pure magnesium in simulated body fluid (SBF) proceeds by an electrochemical reaction with water as shown in Reaction Scheme 1.1. This reaction produces hydrogen gas, magnesium ions and hydroxide ions leading to an increase in pH and ionic strength of the surrounding solution resulting in the precipitation of magnesium hydroxide at the sample surface [19-28].

Reaction Scheme 1.1: General Corrosion Mechanism of Magnesium [28].

Anodic reaction: $Mg_{(s)} \rightarrow Mg^{2+}_{(aq)} + 2e^-$

Cathodic reaction: $2H_2O_{(l)} + 2e^- \rightarrow 2OH^-_{(aq)} + H_{2\,(g)}$

Product formation: $Mg^{2+}_{(aq)} + 2OH^-_{(aq)} \rightarrow Mg(OH)_{2(s)}$

General reaction: $Mg_{(s)} + 2H_2O_{(l)} \rightarrow Mg(OH)_{2(s)} + H_{2\,(g)}$

The film of $Mg(OH)_2$ that is formed on the surface of the metal can provide protection and reduce the corrosion rate of magnesium. However, this film is readily converted into soluble $MgCl_2$ in an aqueous environment containing chloride anions according to reaction scheme 1.2 [29].

Reaction Scheme 1.2: Influence of Anions.

$$Mg(OH)_{2(s)} + 2Cl^- \longrightarrow MgCl_{2(aq)} + 2OH^-_{(aq)}$$

As the hydroxide layer is converted to soluble $MgCl_2$, the underlying substrate is continually exposed to the corrosive media resulting in the occurrence of severe pitting of the substrate.

Moreover, some studies have reported that calcium phosphate can be formed on the surface of the magnesium alloys exposed to both *in vitro* and *in vivo* environments as

shown in reaction scheme 1.3. This reaction is oversimplified in that other ions in solution such as Mg^{2+} and CO_3^{2-} can be substituted into the crystal structure to form calcium and phosphate deficient calcium phosphate species. This has an impact on the composition, crystallinity and stability of the formed calcium phosphate layer. This layer of calcium phosphate can form in direct contact with the surrounding tissue *in vivo* and can improve both the corrosion rate and the biocompatibility of magnesium in physiological solutions [30].

Reaction Scheme 1.3: Precipitation Reactions.

$$10Ca^{2+}_{(aq)} + 6PO_4^{3-}_{(aq)} + 2OH^-_{(aq)} \rightarrow Ca_{10}(PO_4)_6(OH)_{2(s)}$$

1.2.2 Corrosion Prevention

Several strategies to obtain suitable degradation rates for orthopedic biomaterials have been reported. Some of these strategies include using high purity alloys, addition of new alloying elements, surface modification of the alloys, and deposition of protective coatings. Examples of surface modification methods include chemical conversion, laser modification and anodizing. Protective coatings such as electrochemical plating, conversion coatings, hydride coatings, and organic coatings have also been reported [31].

The corrosion resistance of magnesium alloys depends on the alloying elements. For instance, alloying magnesium with aluminum, generally improves the corrosion resistance. The corrosion rate of magnesium alloys decreases rapidly with increasing aluminum content due to the formation of the more noble β-phase [32]. However, the presence of high concentrations of aluminum can be considered toxic for humans. Therefore, it is highly recommended to use magnesium alloys with low concentrations of potentially toxic metals in biomaterial applications. Furthermore, the presence of zinc in magnesium alloys can increase the tolerance limits and reduce the effect of impurities. In addition, it improves strength without reducing flexibility [32-33].

The alloy that was used in this project is AZ31, A and Z correspond to aluminum and zinc, which are present in the alloy with concentrations of 3 % and 1 % in mass

respectively. This alloy has a good combination of suitable mechanical properties, corrosion resistance and low concentration of aluminum to serve as a good model material to study the influence of surface modification on magnesium alloy corrosion rates and bioactivity.

1.3 Protective and Bioactive Coatings on Magnesium Alloy AZ31

Coatings on biodegradable orthopaedic biomaterial implants should fulfill two main purposes: 1. To control the degradation rate of the metal in the body fluids and 2. To be able to induce the formation of a hydroxyl apatite layer on the surface of the implant to promote good adhesion to the bone tissue [34].

In this project, a multi-layered coating consisting of a silica sol-gel under-layer to protect the substrate from corrosion in body fluids was coupled with a mesoporous silica top-layer to enhance the bioactivity of the implanted material. This mesoporous silica top-layer may also be exploited in the future as a drug delivery system.

1.3.1 Silane as a Protective Coating

Creating a barrier between the metal and its physiological environment is the most effective way to prevent corrosion of magnesium and its alloys; this can be done through the formation of a protective coating. The coating must be uniform, well adhered and pore free [31]. The use of silanes to form protective coatings has been successful with other implant materials, therefore we hypothesize that this coating strategy may also enhance the corrosion resistance of magnesium alloys [35].

Many articles have discussed the formation of a covalently bonded protective silica layer on a variety of substrates such as magnesium alloys, aluminum alloys, iron, stainless steel and other metals [36-37]. Different kinds of silanes have been used to prepare the silica coating but alkoxysilane is one of the commonly studied silica sources. These alkoxysilanes include both silanes ($Si(OR)_4$) and organosilanes (molecules with at least one organic functional group attached directly to the silicon atom, $RSi(OR')_3$) [37].

Tetraalkoxysilanes are chemical compound that consists of four alkyl groups attached to silicon through oxygen atoms with the formula $Si(OR)_4$ where R can be either CH_3 or C_2H_5 [37]. The chemical compound with methyl (CH_3) is called tetramethoxysilane (TMOS) and the chemical compound with ethyl (C_2H_5) is tetraethoxysilane (TEOS) [38]. TEOS is the silica source that has been used in this project to prepare the silica coating.

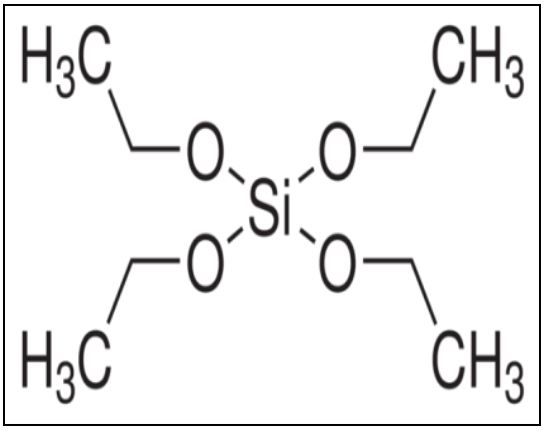

Figure 1-2: The Molecular Structure of Tetraethoxysilane (TEOS).

The methoxy or ethoxy groups of the alkoxysilanes can undergo hydrolysis in the presence of water to form silanol groups. The silanol groups can then condense with hydroxyl groups on the surface to form covalent bonds leading to improve coating integrity and adhesion. In fact, silanes have been commonly used as adhesion promoters between inorganic and organic materials [39].

The most popular method of preparing the silica film is the sol-gel process as it is an environmentally friendly process [40]. Sol-gel coatings have been prepared on many different types of substrates including glass, ceramic, magnesium, aluminum, iron and other metals [40-42]. Compared to other techniques, the sol-gel technique has several advantages that include low cost, excellent adhesion, chemical stability, and good film uniformity. Furthermore, it is a simple deposition procedure at carried out at low sintering temperature [37-42].

The overall sol-gel process consists of two chemical reactions. The first is a hydrolysis reaction and the second is a condensation reaction. The hydrolysis reaction produces the

sol, while the condensation reaction forms a gel on the substrate producing a thin film [43].

The interaction of silane with metal surfaces occurs in two steps according to the sol-gel process. The first step is the hydrolysis of the silane. This occurs when the alkoxy groups react with water to form hydrophilic and reactive silanol groups (Si-OH). An alcohol is released as a side product. The second step is the condensation of silane molecules. In this step the silanol groups can react with each other to form hydrophobic siloxane bonds (Si-O-Si) or they can react with surface hydroxyl groups to form Si-O-Metal bonds. In both cases, water is released as a side product [43-44]. The silane precursor does not need to undergo complete hydrolysis prior to the start of the condensation reaction; the relative rates of hydrolysis and condensation depend on the experimental conditions such as the pH of the solution, the concentration of the silane and the availability of water [45]. At low pH, the rate of hydrolysis of silane molecules is faster than the rate of condensation whereas, at high pH, the rate of hydrolysis is slow and condensation is fast [25]. Moreover, an increase of silane concentration also raises the condensation rate thus influencing the thickness and uniformity of the deposited film [25]. Hydrolyzed silane molecules will react with the surface of metals to form (Si-O-Metal) bonds through hydroxyl groups present at the metal surface [43-44]. The surface coupled silane molecules can further crosslink with each other through Si-O-Si bonds leading to the formation of either a self-assembled monolayer or a multilayer film depending on the reaction conditions [25]. A simplified reaction scheme is shown in reaction scheme 1.4. The reader should keep in mind that molecules with one, two, three or four silanol groups can undergo condensation reactions resulting in a more complex reaction scheme than the one shown here. Furthermore condensation can occur simultaneously between silanol groups or with the surface hydroxyl groups.

Reaction Scheme 1.4: **Silane Chemistry [37-43-45].**

1. The hydrolysis of the silane molecules - (sol formation)

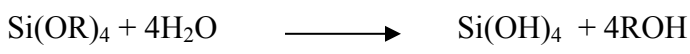

2. The condensation of the silane molecules - (gel formation)

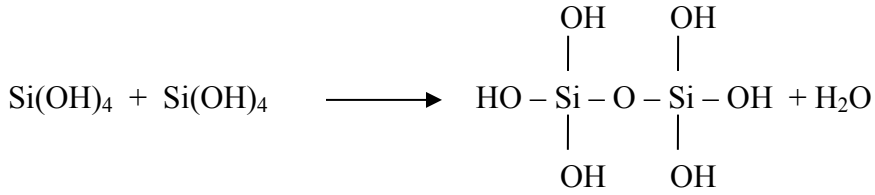

3. The formation of a silane film on metal surfaces

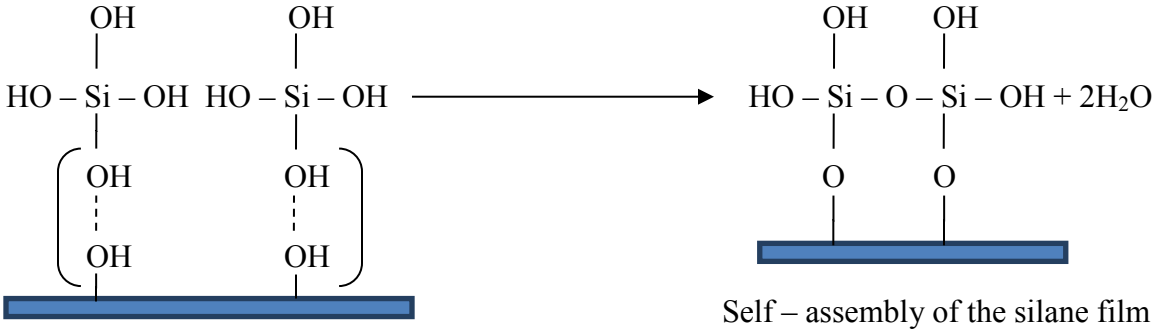

Self – assembly of the silane film

Vasconcelos and his group have demonstrated that sol-gel silica coatings can provide good corrosion protection for stainless steel in a simple salt solution containing 3.5% NaCl [46]. Additionally, previous research has demonstrated that while the sol-gel silica coating has excellent corrosion behavior in simulated body fluid it does not have the ability to induce apatite formation in-vitro [47]. The ability to induce apatite formation is essential for osseointegration of implanted orthopaedic biomaterials. These results suggest that a multi-layered coating consisting of a corrosion resistant silica underlayer coupled with a bioactive top layer would be a good coating for controlling both the degradation rate and bioactivity of magnesium implant materials.

1.3.2 Mesoporous Silica as a Bioactive Coating

1.3.2.1 Overview of Mesoporous Silica Materials

Porous materials have been classified by IUPAC according to their pore size; macropores have a diameter greater than 50 nm, micropores have a diameter less than 2 nm and mesopores have a diameter from 2-50 nm. There are many factors that influence the formation of mesoporous materials such as the starting materials, type of surfactant and reaction conditions (e.g. pH, temperature, solvent, concentration). Mesoporous materials can be either ordered or disordered in a mesostructure. The silica structure is disordered on the atomic scale; however the pore correlation can be well ordered. The pores can have various shapes such as spherical or cylindrical depending on how the materials are synthesized [48].

Mesoporous silica is an inorganic material synthesized in the presence of a surfactant or a block co-polymer, which acts as a template, and a silica precursor molecule. The source of the silica precursor can be sodium silicate or alkoxysilanes such as TEOS or TMOS [49]. Mesoporous silica materials combine the advantages of both silica and mesoporous materials [49-50]. Mobile Crystalline Materials (MCM) was the first family of mesoporous materials synthesized in the early 1990's. These materials were synthesized by Kresge and co-workers in the Mobile Corporation laboratories and include both the MCM-41and MCM-48 materials. These first mesoporous materials were synthesized with a cationic surfactant under basic conditions. In 1998, a new family of mesoporous materials was reported by Zhao et al, these were synthesized with non-ionic tri-block polymers and are named SBA-X (Santa Barbara Amorphous). Other families of mesoporous materials (MSU, FDU, KIT) have since been successfully synthesized using various synthesis conditions and templating agents [51-52]. These include MSU (Michigan State University) materials that are synthesized by a self-assembly mechanism between silica precursors and nonionic poly(ethylene oxide) surfactants [53], FDU which has been synthesized by the Zhao group in FuDan University using various neutral triblock copolymers in acidic media [52] and KIT (Korea Advanced Institute of Science

and Technology) mesoporous silica materials which are also synthesized using triblock copolymers as the mesopore-directing agent under acidic conditions [54].

1.3.2.2 Synthesis of Mesoporous Silica Materials

1.3.2.2.1 Synthesis Conditions

Mesoporous silica materials can be synthesized to have a wide variety of different structural features. It is possible to control the particle size, pore size, pore volume, surface area, morphology and mesoporosity as well as to incorporate different functional groups. These variations allow us to synthesize materials with different physical and chemical properties [55]. The synthesis conditions that affect the structural features are the type of surfactant, the silica source, the ionic strength and pH of the solution as well as the synthesis temperature [56].

The nature of the surfactant plays a particularly important role in the synthesis of mesoporous silica materials. Pore size mainly depends on the chain length of the surfactant, which means that pore diameter increases by increasing the chain length of the surfactant [56-57]. Surfactants are amphiphilic molecules. They are composed of a hydrophilic head and a hydrophobic tail as shown in Figure 1.3 [58]. Surfactants are classified according to their head group which may be cationic, anionic, or nonionic. When the surfactant molecules are immersed in an aqueous solution, the hydrophilic head of the surfactant moves towards the water or the surrounding solvent and they aggregate to form micelles [58]. Examples of surfactants that can be employed in the synthesis of mesoporous silica materials are alkyltrimethyl ammonium bromide (cationic), sodium alkyl sulfate (anionic) and polyethylene oxide, PEO (non-ionic) [51-52]. The surfactant of interest in this project is the cationic surfactant, dodecyltrimethylammonium chloride (DTAC). Its molecular structure is illustrated in Figure 1.4.

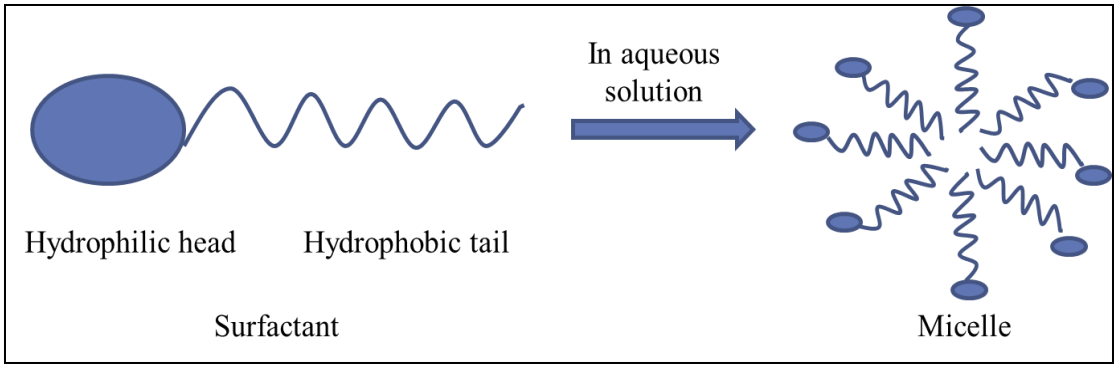

Figure 1-3: Surfactant in Aqueous Solution.

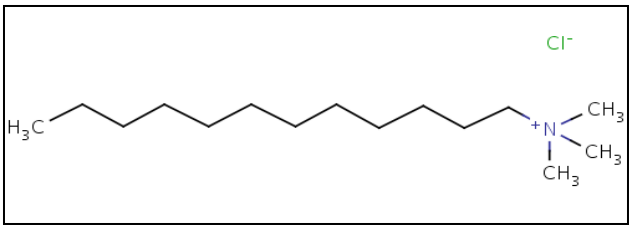

Figure 1-4: The Molecular Structure of Dodecyltrimethylammonium Chloride (DTAC)

1.3.2.2.2 Synthesis Mechanism

Mesoporous silica materials are synthesized through a combination of the sol-gel and self –assembly processes [52]. The mechanism of synthesis for mesoporous silica materials can be described by several steps as shown in Figure 1.5 (adapted from [52]). The first step involves dissolving the silica precursors into an aqueous solution containing surfactant. The silica precursors undergo hydrolysis and condensation to form a sol as described in section 1.3.1. In the second step, the surfactants aggregate to form micelles followed by self-assembly of the hydrolyzed silica molecules on the micelle surface which leads to the formation of silicate-surfactant species. In this way the surfactant micelles act as a template for the formation of the silica particles. In the third step, the silicate-surfactant species complex into ordered arrays as the silane molecules undergo condensation to form silica. Finally, the surfactant must be removed either by calcination or solvent extraction to produce the final mesoporous silica structure [52-55].

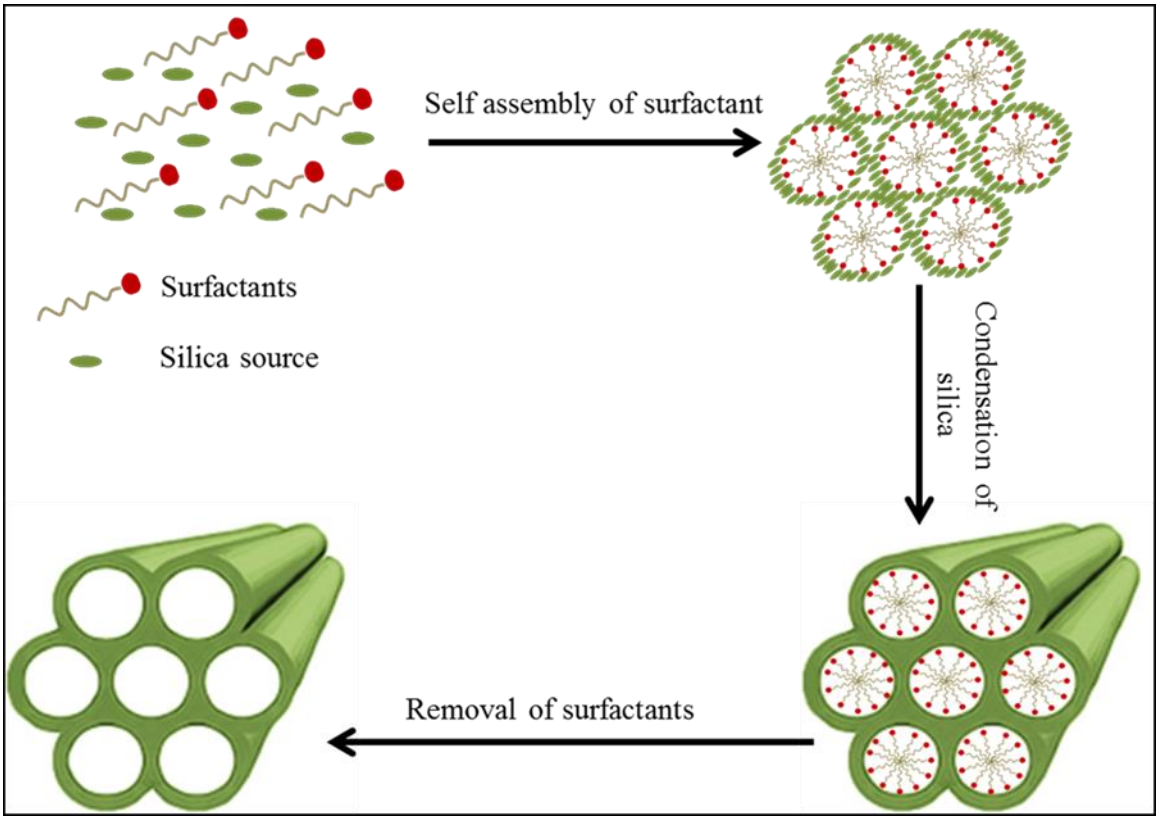

Figure 1-5: The Synthesis Mechanism of Mesoporous Silica Materials. [52]

1.3.2.2.3 Application of Mesoporous Silica Materials

Mesoporous silica materials have received much attention in recent years due to their high surface area, large cumulative pore volume, controllable pore size, morphology, and easy functionalization [59]. Mesoporous silica materials can be synthesized with different pore size by changing the chain length of the hydrophobic group chain in the surfactant template molecule [57] or by using the hydrothermal treatment [52]. Hydrothermal treatment is a post-synthesis treatment done by adding the as-synthesized mesoporous silica materials into an aqueous medium and heating at a particular temperature for a period of time. Post-synthesized hydrothermal treatment has been proposed as an efficient way for pore expansion and for enhancing hydrothermal stability [60]. The overall morphology of mesoporous silica material depends on the type of surfactant used [57]. Moreover, mesoporous silica materials can be functionalized for specific

applications by incorporating different functional groups such as amine (NH_2) and thiol (SH) through an appropriate choice of silica precursor [52].

Mesoporous silica materials are attractive materials for a wide range of applications. They have been studied for use in environmental remediation to adsorb and separate specific elements from aqueous solutions. Several studies have demonstrated that mesoporous silica materials (MCM-41) which were functionalized with thiol, have a high efficiency in terms of removing mercury from aqueous solutions [61-62]. Mesoporous silica materials have also been used in chromatographic columns as a stationary phase for HPLC [63]. Moreover, mesoporous silica materials have shown promise for use in chemical or biological catalysts due to their high surface area which leads to increased reaction rates. Other potential applications include nanotechnology, functional devices (as a sensor), and biomedical applications such as drug delivery and bone regeneration [63].

1.3.2.2.4 Biomedical Applications of Mesoporous Silica Materials

Mesoporous silica materials have begun to attract attention for biomedical applications due to their high surface areas, high pore volumes, and good biocompatibility.

A growing area of application for these materials is their application as a biomaterial that promotes bone tissue regeneration. In recent years, studies have shown that mesoporous silica materials are suitable for use as starting materials for bone tissue engineering technologies due to their outstanding properties and biocompatibility [64-65]. The nanostructure of these materials is believed to be responsible for their ability to promote new bone formation; this is evidenced by:

1. The formation of apatite layers on their surface in simulated body fluid which indicates that they are bioactive.
2. The stimulation of osteoblast proliferation and differentiation which accelerates the healing process [64].

Izquierdo-Barba, et al. (2005), have reported the formation of an apatite-like layer on the mesoporous silica materials SBA-15 and MCM-48 that were soaked in simulated body fluid [56]. In addition, another group of researchers demonstrated that osteoblast proliferation was promoted by mesoporous silica materials in the early stages of cell attachment. They also indicated that an increase in the surface area led to an increase in serum protein adsorption and a faster apatite layer formation rate [66]. Recently, Lozano, and his research group have shown that both unmodified and organically modified SBA-15 materials loaded with osteostatin, a parathyroid hormone-related protein (PTHrP) that is an important regulator of bone formation and remodeling, increased cell proliferation and the expression of several osteoblastic products [67].

Furthermore, a study by Katiyar et al. has demonstrated that protein was adsorbed on mesoporous silica when these materials were immersed in bovine serum albumin (BSA). BSA loading tests have shown that there is a direct dependence of protein adsorption on pore size: the greater the pore diameter, the higher the amount of protein loading [68].

In addition, several research groups have established that cell uptake and cellular toxicity of the mesoporous silica materials are influenced by the particle's size, shape, surface charge and functional groups. However, other studies have concluded that no cytotoxicity is detected up to 100 $\mu g\ mL^{-1}$ for non-modified 100 nm mesoporous silica particles; this is well above the effective concentrations required for most healing treatments [69]. Possible toxicity and the mechanism of excretion of mesoporous silica materials *in vivo* were also investigated by injecting mesoporous silica particles into a live mouse tail. The test subjects did not show any evidence of toxic effects during the one month study and the particles of silica were excreted in the urine [55].

In addition to their potential application for bone healing, mesoporous silica materials have shown promise as drug delivery-systems [70]. There are numerous examples of drug molecules that have been incorporated into mesoporous silica materials. In 2001, Vallet-Regi and co-workers were the first researchers that reported the use of mesoporous silica materials (MCM-41) as delivery matrices for ibuprofen (an anti-inflammatory drug) [71-72]. This led to significant interest in using these materials for drug delivery and

several different types of drugs have been successfully loaded into the pores such as amoxicillin, gentamicin, aspirin, and erythromycin. The influence of the pore size of the mesoporous silica materials on drug delivery rates has also been investigated. The results indicated that the delivery rate of ibuprofen in SBF solution decreases as the pore size decreases and the higher the surface area, the higher the amount of drug loaded [73]. Furthermore, mesoporous silica materials have been effectively used for the delivery of anticancer drugs [65]. Moreover, they are one of the most promising drug delivery materials in orthopedic surgery; they have been used as implantable drug delivery devices for bone tissue to help the healing process by loading antibiotics, growth factors, chemotherapeutic agents, antiestrogens, and anti-inflammatory drugs to prevent inflammation [71].

1.3.2.3 Mesoporous Silica Materials as an Implant Coating

Mesoporous silica materials have been used as a biomaterial coating on different substrates such as titanium, glass and stainless steel due to its biocompatibility and its ability to be used as a multifunctional implant coating.

The biocompatibility of mesoporous silica materials have been confirmed by several researchers as discussed in the previous section (1.3.2.2.4). In summary, previous publications have shown the biocompatibility of mesoporous silica coatings in several ways. The first one involves the formation of hydroxyapatite on its surface which is the essential condition for a material to bond with living bone (bioactivity). Gomez-Vega et al, (2001) have indicated that mesoporous silica coatings on different substrates (glass, silicon, and titanium), can form apatite when they are immersed in a stimulated body fluid [74]. The same authors report a multi-layer coating strategy that consists of a mesoporous silica film as a second layer on titanium to enhance the bioactivity while using a thick glass coating to protect the substrate from corrosion [75]. The second evidence of biocompatibility involves the stimulation of osteoblast adhesion, proliferation and differentiation which accelerates the healing process. Wang et al, (2010) used a mesoporous bioactive glass coating on stainless steel to improve implant-bone integration. The authors reported that the mesoporous structure of the coating was

responsible for protein adsorption followed by osteoblastic cell attachment, proliferation and differentiation [76]. The third evidence of biocompatibility is the non-toxicity and non-inflammatory effect to the tissues that was demonstrated by several research groups [55-69].

In addition to their biocompatibility, mesoporous silica can be used as a multifunctional implant coating that acts as a bioactive coating for inert materials and a surface drug delivery system at the same time. An example of this is in the incorporation of antibiotics into mesoporous silica coatings deposited on implant materials.

Infection is the most common serious problem associated with medical implants after surgical implantation. To prevent infection and inflammation, patients usually take antibiotics and anti-inflammatory medications orally, intravenously, intramuscularly or topically. However, drugs administered via these routes cannot easily reach the implant/tissue interface. Thus, local drug delivery has become a common way to eliminate the risk of obtaining infection after implant surgery [77]. For this reason, Ehlert and his co-worker have successfully developed a local drug delivery and bioactive coating on glass by using mesoporous silica that was loaded with the antibacterial drug ciprofloxacin to prevent bacterial infections after implantation [78].

1.4 Objectives of the Thesis

In recent years, magnesium and its alloys have been introduced as a new material of interest in the biomaterials research community. They are of particular interest for use as an orthopaedic biomaterial due to their excellent biocompatibility, biodegradability, and their mechanical properties which are similar to natural bone. One of the major problems preventing the widespread use of magnesium alloys is poor corrosion resistance in physiological solutions. This decreases the mechanical integrity of the implants in the early stages of healing and has a negative impact on the overall biocompatibility. Therefore, protective and bioactive coatings are required to improve their corrosion resistance and provide optimum biocompatibility in order to achieve ideal degradation rates and to maintain the mechanical integrity of the implant during the initial stages of

implantation. The use of silanes as protective coatings has been successful with other implant materials such as aluminum alloys and steel so the study with magnesium alloys may be beneficial as well. Mesoporous silica materials have been shown to have good bioactivity and the ability to stimulate osteoblast proliferation and differentiation at implant surfaces. Furthermore, they have been shown to be non-toxic and non-inflammatory to mammalian tissues. Several studies have shown that mesoporous silica coatings can be deposited on a variety of different substrates including: titanium, glass, and stainless steel.

Therefore, the specific objectives of this project are to:

1. To develop a method for depositing a multi-layered bi-functional coating consisting of a sol-gel silica protective pre-layer followed by a bioactive mesoporous silica film on magnesium alloy AZ31.

2. To optimize the coating conditions and to characterize the surface chemistry, structure and bioactivity of the deposited coatings.

3. To study the impact of the deposited coatings on the corrosion resistance of the magnesium substrate in simulated body fluid (SBF).

Chapter 2

2 « Materials and Methods »

2.1 Materials

Disks of magnesium alloy AZ31 (Alfa Aesar) were used in this project as a substrate, the composition of the material is listed in Table 2-1. The materials used for polishing were purchased from Buehler Canada and included; 320 grit P400 sandpaper, Texmet® 1000 polishing pads, oil-based lubricant and 9, 3, and 1 micron MetaDi® oil-based diamond slurries. A list of chemicals and their basic properties used in this study is given in Table 2-2. For the corrosion test, magnesium alloy AZ31 disks were mounted in an epoxy resin; a mixture of Buehler's EpoxiCure Epoxy Resin and EpoxiCure Resin Hardener. Hanks balanced salt solution was employed as the medium used for both the corrosion test and evaluation of the bioactivity (Table 2-3).

Table 2-1: The Composition (% mass) of Magnesium Alloy AZ31.

Alloy	**Mg**	**Al**	**Zn**	**Mn**	**Si**	**Cu**	**Ni**	**Fe**
AZ31	Bal.	3.0	1.0	0.43	0.01	<0.01	<0.001	0.003

Table 2-2: Table of Chemicals.

Compound	**Molecular Formula**	**Molecular Weight (g/mol)**	**Density (g/mL)**	**Boiling Point (^{o}C)**
TEOS	$SiC_8H_{20}O_4$	208.33	0.933	166-169
DTAC	$C_{15}H_{34}ClN$	263.89	N/A	N/A
Methanol	CH_3OH	32.04	0.7918	64.7
Acetone	CH_3COCH_3	58.90	0.79	56.3
Deionized Water	H_2O	18.02	1.00	100
Sodium Hydroxide	NaOH	40.00	2.1	318
Nitric Acid	HNO_3	63.01	1.5129	109
Ammonia	NH_4OH	35.04	0.91	37.7

Table 2-3: The Composition of Hanks Balanced Salt Solution.

Component	**Concentration (g/L)**
$CaCl_2$. $2H_2O$	0.185
$MgSO_4$ (anhyd)	0.09767
KCl	0.4
KH_2PO_4(anhyd)	0.06
$NaHCO_3$	0.35
Na_2HPO_4(anhydrous)	8.0
D-Glucose	0.04788

2.2 Methods

An overview of the experiments conducted and the experimental method used in this thesis is shown in Figure 2.1. In brief, the magnesium alloy AZ31 samples were polished, cleaned and alkaline aged. A multi-layer coating was then deposited on the substrate by dip coating. The first layer was a sol-gel silica to protect the sample from corrosion. The second layer was a mesoporous silica layer to enhance the bioactivity of the material. The coating chemistry and morphology were characterized by infrared spectroscopy, scanning electron microscopy/energy dispersive spectroscopy analysis and atomic force microscopy. The corrosion resistance and bioactivity of the coated samples were evaluated via an immersion test in simulated body fluid. Details for each stage of the experimental procedure are given in the sections below:

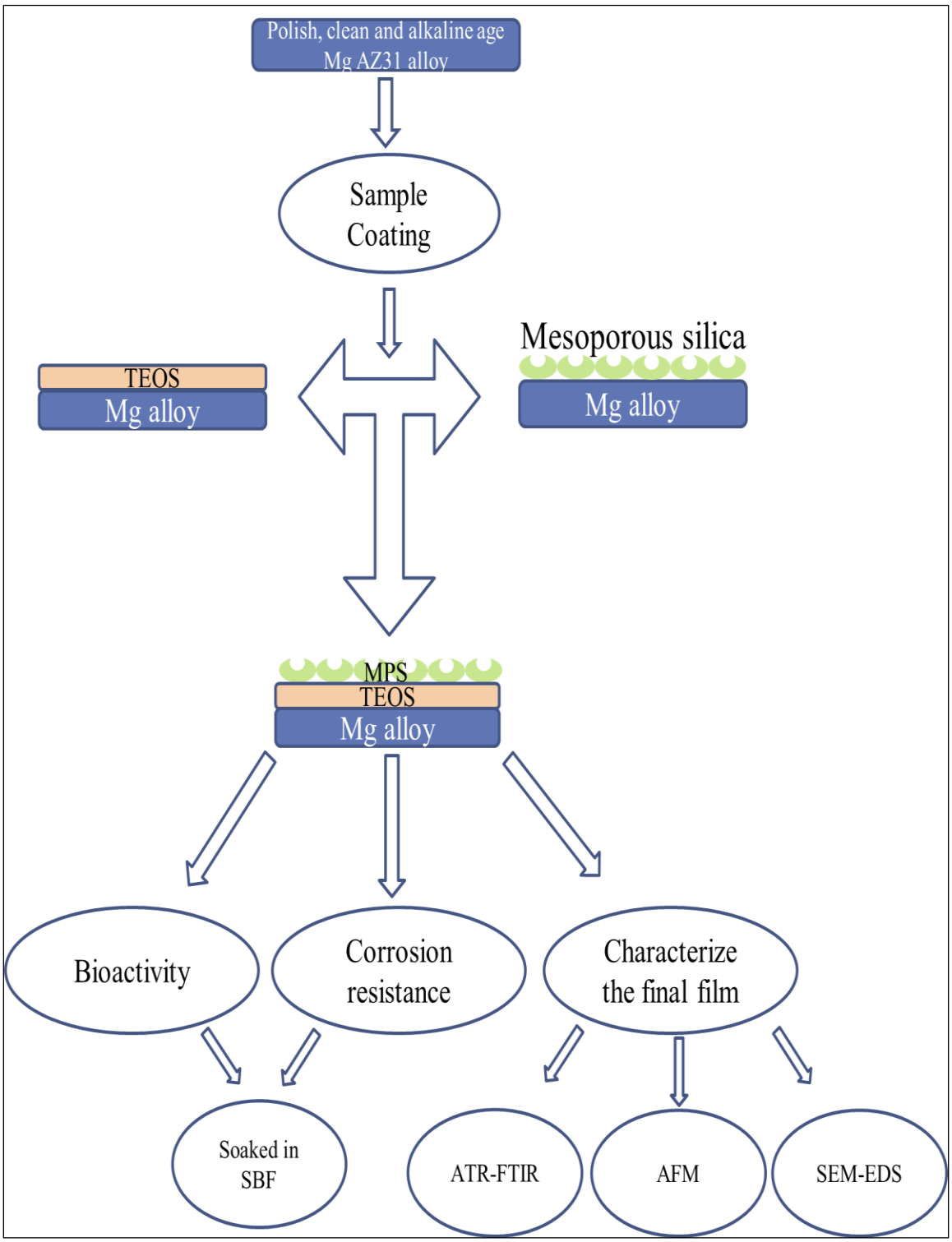

Figure 2-1: An Overview of the Experimental Procedure.

2.2.1 Polishing AZ31 Mg Alloy

The AZ31 magnesium alloy samples were polished to a one micron surface finish in order to remove the gross oxide layer. The samples were polished in a series of steps. The first step was polishing the samples with a 320 Grit P400 sand paper and oil-based lubricant. The next step involved polishing the samples with a finer pad using a 9 micron diamond suspension for six minutes, followed by a 3 micron diamond suspension for five minutes and finally a 1 micron diamond suspension for four minutes. The samples were rinsed with water between each step.

2.2.2 Cleaning

In order to remove any excess polishing oil from the surface of the alloys, they were cleaned with a three step process. In the first step, they were sonicated in acetone for 20 minutes. In the second step, they were rinsed in deionized water for 30 seconds. Finally the samples were air dried.

2.2.3 Alkaline Aging

The formation of hydroxyl group on the surface is very important for the covalent bond formation between the metal and the sol-gel silica coating. Therefore, the samples were immersed into an alkaline bath (0.05M NaOH, pH 12.5) at 50 °C for one hour to promote the formation of surface hydroxyl groups.

2.2.4 Coating Procedures

2.2.4.1 Sol-gel Silica as a Pre-layer

The silane coating solutions were prepared by using methanol as the solvent, deionized water, ammonia, and TEOS in varying v/v ratio as shown in Table 2.4. The solution was allowed to stir for 24 hours to ensure complete hydrolysis before coating.

Table 2-4: Sol-Gel Silica Coating Solution Composition

Coating Solution%	TEOS (mL)	Methanol (mL)	Deionized Water (mL)	Ammonia (mL)
3.2	3.2	76.8	14	6
1.6	1.6	78.4	14	6
0.8	0.8	79.2	14	6
0.4	0.4	79.6	14	6

The samples of AZ31 Mg alloys were immersed into 40 mL of the solutions that were prepared using various concentrations of TEOS. The studied concentrations were 0.4, 0.8, 1.6 and 3.2% (v/v) of TEOS/Solvent. The coating process was optimized at different deposition times (20 min, 1, 4 and 24 h) to determine the best coating conditions for stable and uniform silane films on the surface of the magnesium alloy. After coating, the samples were dried before curing in an oven for 1h at 100 °C.

2.2.4.2 Deposition of Mesoporous Silica Multilayers

The mesoporous silica coating solutions were prepared by using TEOS as a silica precursor and the cationic surfactant C_{12}TAC (Dodecyltrimethylammonium chloride) as the templating agent in deionized water, methanol, and ammonia as the solvent. The coating solution was prepared according to [79] with a molar ratio of TEOS: C_{12}TAC: deionized water, methanol, and ammonia was 1:0.4:774:1501:72. Therefore, 100 mL of methanol was mixed with 0.248 g of C_{12}TAC, 17.7 mL of deionized water, 8 mL of 28% aqueous ammonia solution and 0.368 mL of TEOS. The solution was hydrolyzed for 1h prior to immersion of the magnesium alloy samples.

The sol-gel silica coated samples were deposited into the mesoporous silica solutions for different deposition times (20 min, 1, 4 and 24 h). In some cases, multiple layers of mesoporous silica were deposited by successive immersion of a sol-gel silica coated sample in fresh mesoporous silica coating solution. The samples were washed with methanol and air dried after each successive layer was deposited. The final coated

specimens were cured in an oven at 100 °C for 1 h. After curing, the samples were calcined at 350 °C for 3 h followed by gradual cooling of the samples down to room temperature in order to remove the surfactant.

2.2.5 Corrosion Test

2.2.5.1 Mounting the Discs in Epoxy

The samples were mounted in epoxy to ensure a uniform surface area and surface chemistry for the corrosion test. This was done by mixing five parts of Buehler's EpoxiCure Epoxy Resin with one part Epoxicure Resin Hardener for around three minutes until the mixture became clear. The mixture was allowed to set for 30 minutes until a higher viscosity was achieved. Then the mixture was dropped onto parafilm that had been pre-coated with a release agent to facilitate its removal and the coated samples were placed into the epoxy and allowed to set overnight. The parafilm was removed prior to corrosion testing.

2.2.5.2 Corrosion Test

The coated samples were immersed into 25 mL of Simulated Body Fluid (SBF) (Table 2-3). The samples were stored at 37 °C to mimic *in vivo* conditions. To compare the corrosion rates of the coated samples to the uncoated magnesium alloy, the concentration of magnesium ions was measured as a function of time by flame atomic absorbance spectroscopy. The solutions were changed daily over a one week period. For each sample, a 100 µL aliquot was taken from the corrosion medium and diluted to 10 mL with 2% HNO_3 in a volumetric flask. Finally, the corroded samples were removed from the solution after seven days and they were rinsed with deionized water. The samples were dried prior to further analysis.

2.2.6 Bioactivity Test

The test was done under the same conditions as the corrosion test described in the previous section (2.2.5.2). However, the samples for characterization of the bioactivity

were removed from the SBF at different times (1, 3 and 7 days) in order to examine them for their ability to induce calcium phosphate formation at the surface. The surface chemistry and morphology after immersion in SBF was examined by ATR-FTIR and SEM/EDS.

2.2.7 Instrumental Analysis

2.2.7.1 Attenuated Total Reflectance – Fourier Transform Infrared Microscopy (ATR-FTIR)

Attenuated Total Reflection Fourier Transform Infrared microscopy (ATR- FTIR) was used to analyze the surface of the coated samples after each step. A Bruker Optics Hyperion infrared microscope was employed. The main goal of this technique was to determine the chemical functional groups present on the surface of the coated magnesium alloys. The spectra were taken in three spots for each sample and were corrected with the atmospheric compensation function of the software to remove water vapour and CO_2 from the spectra. The determination of the stability and uniformity of the film was also determined using this technique. The uniformity was measured by integration of the area underneath the peaks for 3 spots on each sample. Larger peak areas were correlated with an increase in film thickness at a given location on the sample. Large spot to spot standard deviations were assumed to correlate with non-uniformity. The peak chosen for this study was the Si-O peaks between 1050 and 1250 cm^{-1} since they did not overlap with any substrate peaks. Furthermore, ATR-FTIR was employed for the identification of the corrosion products on the surface of the samples after immersion in SBF.

In this technique, IR radiation undergoes total internal reflection through an ATR crystal which has high refractive index. The total internal reflection results in the formation of an evanescent wave, which penetrates into the sample in contact with the crystal. The evanescent wave decays exponentially away from the interface making this technique somewhat surface sensitive. The resulting spectrum can be used to determine the chemical functional groups on the surface [80].

2.2.7.2 Atomic Force Microscope (AFM)

Atomic force microscope is one type of scanning probe microscope which is used to image the topography of surfaces at high resolution and measure the surface forces. Atomic force microscope (AFM) was used for characterization of the surface morphology of the deposited mesoporous silica coatings. In this research, a Bruker multimode AFM III D was used to capture the images in tapping mode. Bruker AFM TESPA probes with a resonant frequency of approximately 320 KHz were used. An image area of 5 μm x 5 μm was scanned at a scan rate of 0.5 Hz and 512 samples/line.

2.2.7.3 N_2 Adsorption/Desorption

This technique allows determination of the specific surface area of a sample based on the adsorption of nitrogen. This theory is also known as Brunauer-Emmett-Teller (BET). The BET gas adsorption method has become the most commonly used for the determination of the surface area of porous materials.

The BET (Brunauer, Emmett and Teller) equation is [81]:

$$\frac{\frac{P}{P_0}}{n_a\left(1-\left(\frac{P}{P_0}\right)\right)} = \frac{1}{n_m \cdot C} + \frac{C-1}{n_m \cdot C} \cdot \frac{P}{P_0}$$

Where are n_a = adsorbed amount, n_m = monolayer capacity and C = BET constant.

The IUPAC classify the adsorption isotherms in six types shown in Figure 2.3 (adapted from [80]). The adsorption isotherms are presented as the amount of gas adsorbed on the solid plotted versus the relative pressure. The Type I isotherm describe the adsorption behavior of microporous adsorbents. Type II isotherms characterize a non-porous or macroporous adsorbent. Type III presents adsorption on a macroporous adsorbent with weak adsorbate-adsorbent interaction. Type IV isotherms are typically observed for mesoporous materials. The observed hysteresis loop is associated with capillary

condensation within the mesopores. Type V isotherms also have a hysteresis loop and they represent adsorption on porous adsorbents with weak adsorbate-adsorbent interactions. Finally, type VI isotherms represent stepwise multilayer adsorption that is obtained on a uniform non-porous surface [82].

Hysteresis loops are indicative of how the pores are shaped. There are four types of hysteresis loops as shown in Figure 2.3 (adapted from [81]). Type H1 is associated with uniform spherical particles that have a narrow distribution of pore size. Type H2 represents porous adsorbents but the distribution of pore size and shape is non-uniform. Type H3 is associated with aggregates of plate-like particles that give slit-shaped pores. Type H4 is similar to type H3 and is associated with slit-like pores with a narrow pore size [82].

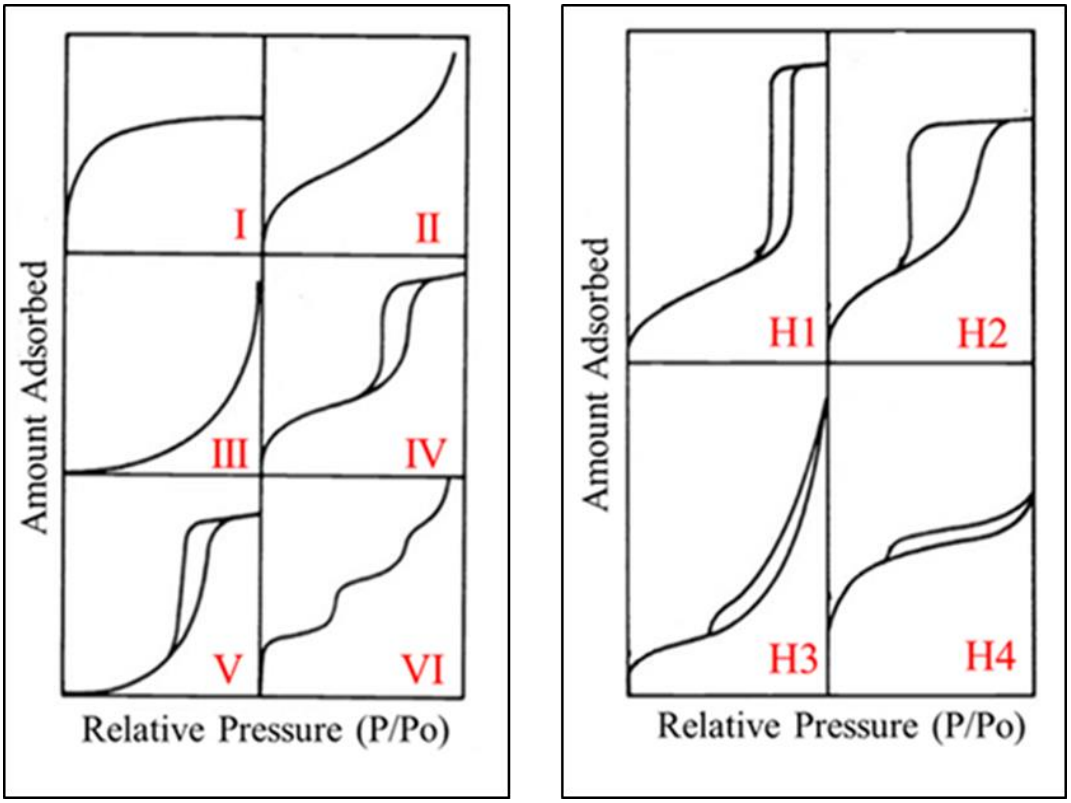

Figure 2-2: IUPAC Isotherms Types and Types of Hysteresis Loops. [81]

2.2.7.4 Flame Atomic Absorption Spectroscopy (FAAS)

Flame atomic absorption spectroscopy (FAAS), a Perkin Elmer AA analyst 400, was used to compare the corrosion rate of the coated magnesium alloys to the uncoated material. This technique was used to measure the concentration of magnesium ions that have been released into the solution during the corrosion test. The concentration measurements were done by using a calibration curve for standards of known concentrations of magnesium (0.05, 0.1, and 0.2 mg/L). An SBF control set was used to compare the concentrations of magnesium ions in the SBF solution with the solutions that had been exposed to the coated and uncoated magnesium alloy.

2.2.7.5 Scanning Electron Microscopy-Energy Dispersive X-ray Spectroscopy (SEM-EDS)

Scanning electron microscopy and energy dispersive X-ray spectroscopy (SEM-EDS) was used to evaluate the surface morphology and texture of the samples after immersion in simulated body fluid. SEM images were obtained using a digital scanning electron microscope (JEOL 6400). Energy Dispersive X-ray Spectroscopy (EDS) was used to determine the elemental composition of the sample surface. Samples to be analyzed were coated with a thin film of carbon to render the sample conductive. The Oxford EDS was operated at 20 kV and the beam current of the electron gun was 1 nA.

Chapter 3

3 « Results and Discussion »

3.1 Optimization of Sol-gel Silica Pre-layer Coating Conditions

The study of the influence of varying TEOS concentration and deposition time is an effective way to optimize the coating conditions for sol-gel silica films deposited on Mg alloys. This optimization process allowed us to choose appropriate conditions to produce sol-gel silica films with the best uniformity and thickness. The coated samples were analyzed by infrared analysis to estimate the variation of thickness and uniformity of the sol-gel silica films on the surface. Spectra were collected (3 spots/sample) for magnesium alloys coated with solutions containing various TEOS concentration at different deposition times. The studied concentrations were 0.4, 0.8, 1.6 and 3.2% of TEOS (v/v, TEOS/Solvent). The deposition times studied were 20 min, 1, 4 and 24 h. The variation in thicknesses as a function of coating conditions has been estimated by integration of the area under the peaks of interest. The size of the error bars (spot to spot variations) associated with these measurements has been used to estimate the overall uniformity of the deposited coatings. The peak chosen for integration, since they are unaffected by any absorptions from the substrate, were the Si-O peaks (1050-1250 cm^{-1}).

3.1.1 Control Sample of Magnesium Alloy AZ31

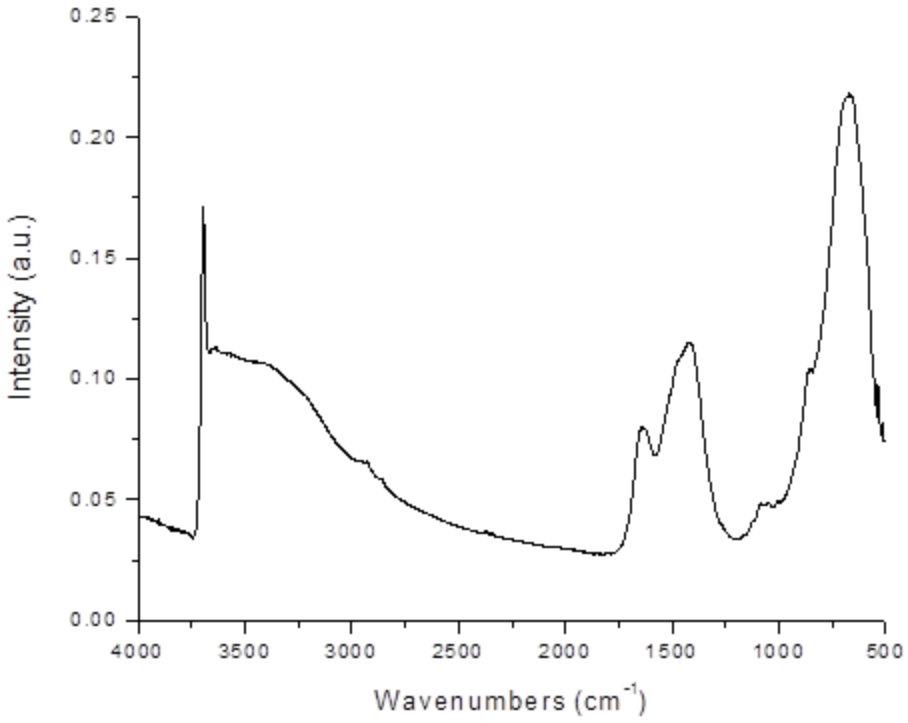

Figure 3-1: IR Spectrum of Mg alloy AZ31 after Surface Pretreatment.

The surfaces of the magnesium alloy samples were prepared, as described in the methodology section. An ATR-FTIR spectrum for a polished, cleaned and alkaline aged sample is shown in Figure 3.1. This spectrum has a sharp peak at 3700 cm^{-1} (O-H stretch) which indicates the presence of crystalline $Mg(OH)_2$. A broad peak up to 3000 cm^{-1} (O-H stretch) was also observed coupled with a peak at 1640 cm^{-1} (O-H bend). Together, the presence of these two peaks shows that there is either surface adsorbed water and/or non-crystalline magnesium hydroxide on the surface. Carbonate (CO_3^{2-}) is also observed (1450 cm^{-1}) due to the reaction of the magnesium substrate with carbon dioxide in the atmosphere. Furthermore, it can be observed that despite the extensive cleaning regimen, peaks at 2850-2930 cm^{-1} (CH_2/CH_3 stretch) indicating that organic contamination is still present on the surface due to adsorption of adventitious carbon from the atmosphere.

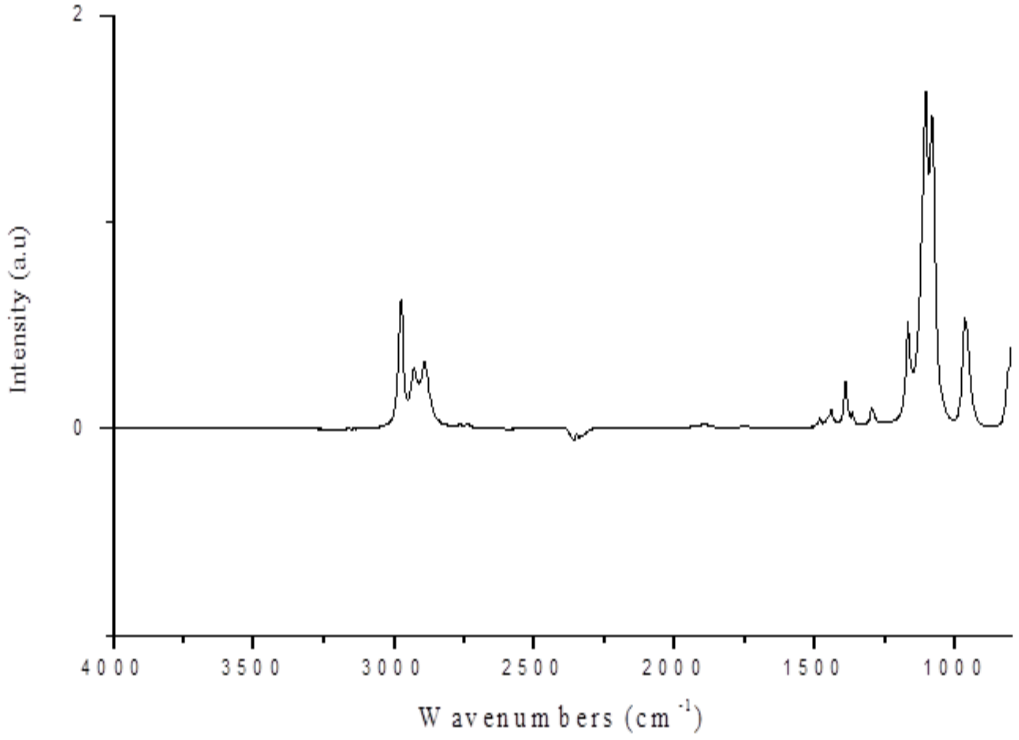

Figure 3-2: IR Spectrum for TEOS.

A reference spectrum for pure TEOS is shown in Figure 3.2. Several peaks of particular interest have been used to confirm the hydrolysis and condensation of TEOS in the sol-gel silica coating on the surface of magnesium alloys. Two regions of particular interest are the Si-O stretch at 1050-1250 cm^{-1} and the peaks at 2850-2930 cm^{-1} which are attributed to the CH_2/CH_3 stretch of the ethoxy groups of the unhydrolyzed silane. On the coated samples (Figure 3-3) the peaks at 2850-2930 cm^{-1} have disappeared indicating that hydrolysis has occurred and that the coating does not contain unhydrolyzed alkoxy groups. Furthermore, the Si-O stretch from 1050-1250 cm^{-1} has significantly broadened due to condensation of the hydrolyzed silane molecule to form Si-O-Mg and Si-O-Si bonds. These peaks were chosen because they occur in regions of the infrared spectrum where there is no interference from peaks due to the substrate.

3.1.2 Study on the Influence of TEOS Concentration

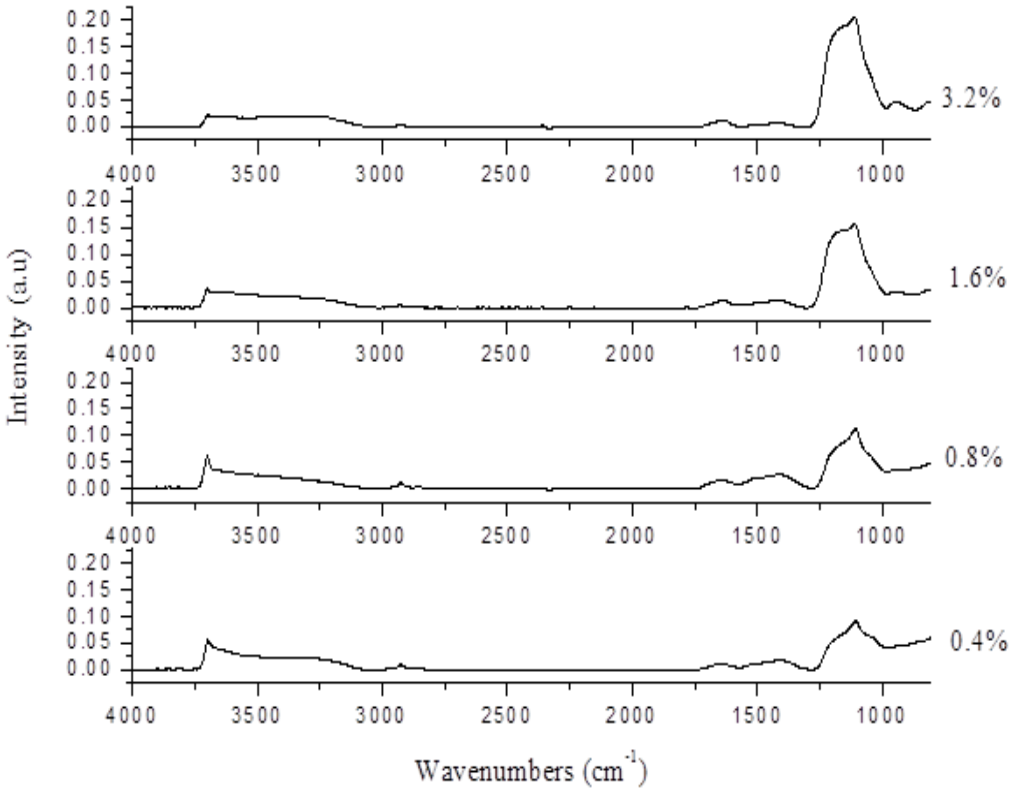

Figure 3-3: IR Spectra for Sol-gel Silica Coating on Magnesium Alloy AZ31 at Various Concentrations of TEOS.

Figure 3.3 shows representative infrared spectra for magnesium alloy AZ31 disks coated with sol-gel silica prepared with various concentrations of TEOS at a constant coating deposition time of 20 minutes. The peaks that are indicative of the presence of sol-gel silica coating were observed in all of the spectra. The common difference in these spectra is the intensity of the peaks. As shown in the figure, the intensity of Si-O peaks increase with an increase in TEOS concentration in the coating solution. It is also observed that the intensities of the peaks due to the substrate ($Mg(OH)_2$ at 3700 cm^{-1} and O-H bond at 1640 cm^{-1}) decrease with increasing concentration. This increase in peak intensity for TEOS peaks coupled with a decrease in the intensity of the substrate peaks indicates that the thickness of the coating increases with an increase in TEOS concentration in the

coating solution. The peak at 3700 cm^{-1} can be attributed to the presence of either Mg-OH or silanol (Si-OH) peaks. However, in this instance the identity of this peak was confirmed to be crystalline Mg-OH from the substrate since it was completely unaffected even after thermal treatment for 24 hours. If this peak were due to Si-OH groups, thermal treatment would have resulted in further condensation of the Si-OH groups in the coating and a concomitant decrease in the peak at 3700 cm^{-1}.

3.1.3 Study on the Influence of Deposition Time of TEOS

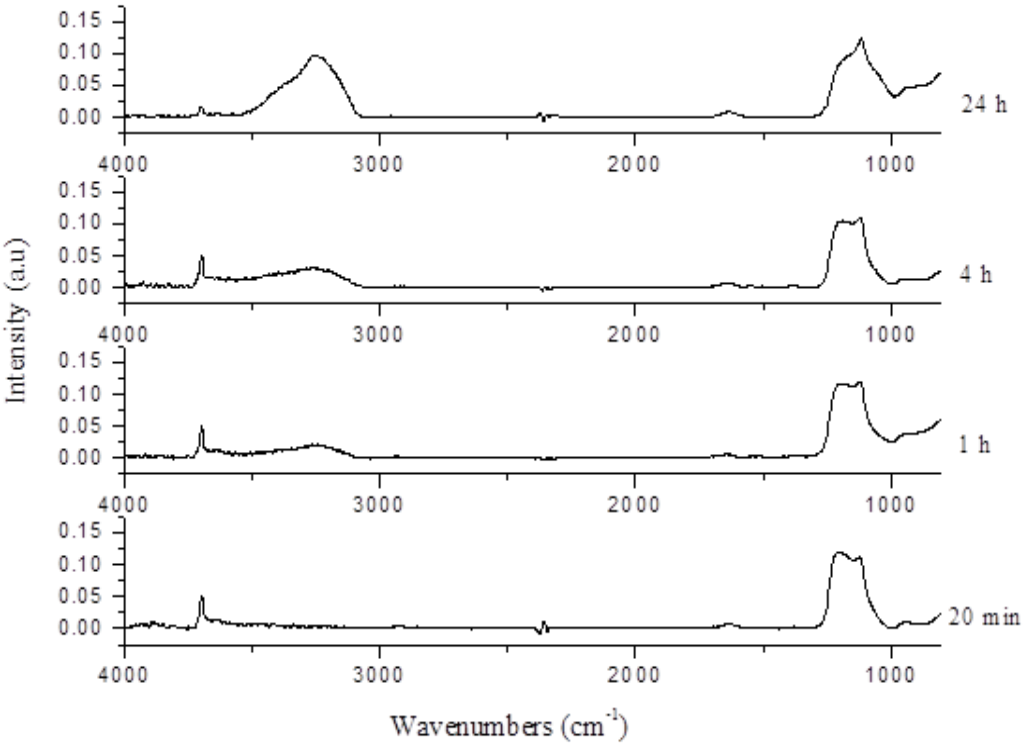

Figure 3-4: IR Spectra for Mg Alloy AZ31 Coated with 3.2% TEOS at Various Deposition Times.

Figure 3.4 shows representative infrared for samples prepared from 3.2% TEOS solution as a function of deposition time. It is clear from the figure that the intensity of the Si-O peak does not increase with the increasing deposition time from 20 min to 4 h. However, the spectrum for long deposition time (24 h) shows an increase in the silicate peak

intensity as well as a decrease in the intensity of the magnesium hydroxyl peaks at 3700 cm^{-1}, indicating an increase in the thickness of sol-gel silica film. However, Figure 3.5 demonstrates that the films deposited at long deposition time are non-uniform. This will be discussed in more detail in section 3.1.4 below.

3.1.4 Study on the Influence of the Deposition Time and TEOS Concentration on Thickness and Uniformity of the Sol-gel Silica Coating

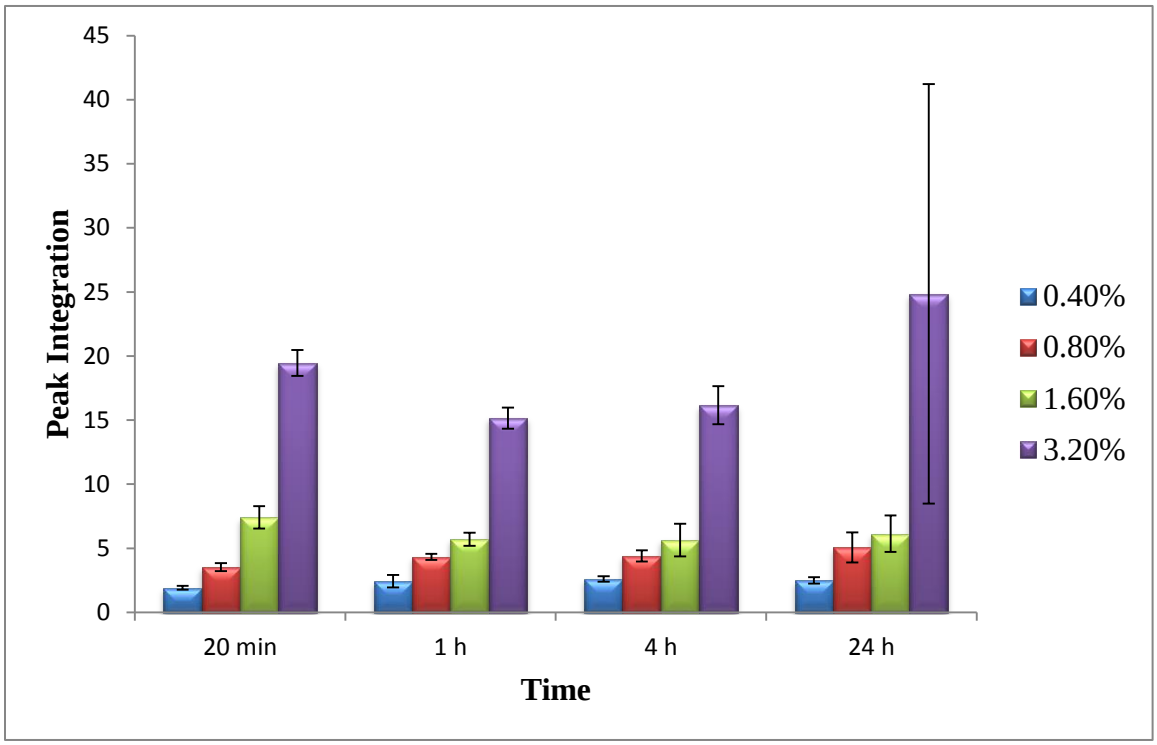

Figure 3-5: Graph of Silica Peak Areas as a Function of Deposition Time and Concentration of TEOS.

Figure 3.5 is a graph showing the average integrated area under the Si-O peak as a function of TEOS concentration and deposition time. The error bars are the spot to spot standard deviation in the area under the peak for each sample. Although it is impossible to exactly reproduce the contact area of the ATR crystal with the sample surface for each measurement, the error bars for 9 different measurements for each sample type are relatively small. This suggests that the trend we have observed is real although an actual quantitative value cannot be obtained. This graph indicates that there is an increase in

sol-gel silica coating thickness as a function of TEOS concentration in solution. These results further demonstrate that the deposition time does not have a significant effect on the thickness of the sol-gel silica coating. However, long deposition times coupled with higher TEOS concentration (24 h, 3.2% TEOS) was observed to result in film non-uniformity as evidenced by the large error bar for this sample. This non-uniformity of the film may be due to the reaction conditions. At high concentrations and extended deposition times, the condensation reaction between hydrolyzed silane molecules in solution may be favoured over condensation of the molecules with surface hydroxyl groups. This would result in the formation of oligomers in the solution which subsequently attach to the surface rather than multilayer deposition directly at the solution/substrate interface.

From the results obtained, it is clear that the optimum conditions for deposition of the sol-gel silica protective pre-layer on Mg alloys are high TEOS concentration (3.2% v/v) and low deposition time (20 min.) since this gives films with both a maximum thickness and good uniformity.

3.2 Deposition of Mesoporous Silica as a Bioactive Coating

In order to ensure that magnesium alloys can promote bone re-growth, it is very important to ensure that the surface modified material has the ability to induce the formation of a hydroxyl apatite layer on its surface. Therefore, the second part of this project was to deposit a mesoporous silica coating on magnesium alloy AZ31 to improve the bioactivity.

3.2.1 Optimization of Mesoporous Silica Coating Conditions on Bare Magnesium Alloy AZ31

To determine the best coating condition for mesoporous silica coatings that were uniform, stable, and had the ability to form hydroxyapatite on its surface, the effect of varying the coating deposition time and the number of treatments (dip coatings) was studied. The coated samples were analyzed by infrared microscopy to compare the

thickness and uniformity of the mesopourous silica films on the surface of magnesium alloys after immersion in the mesoporous silica solution for 20 min, 1, 4 and 24 h. The influence of calcination on the as-deposited mesoporous silica films was also studied by infrared microscopy. Atomic force microscope (AFM) was used for the characterization of surface morphology of mesoporous silica coatings as a function of the number of treatments or dips in the coating solution.

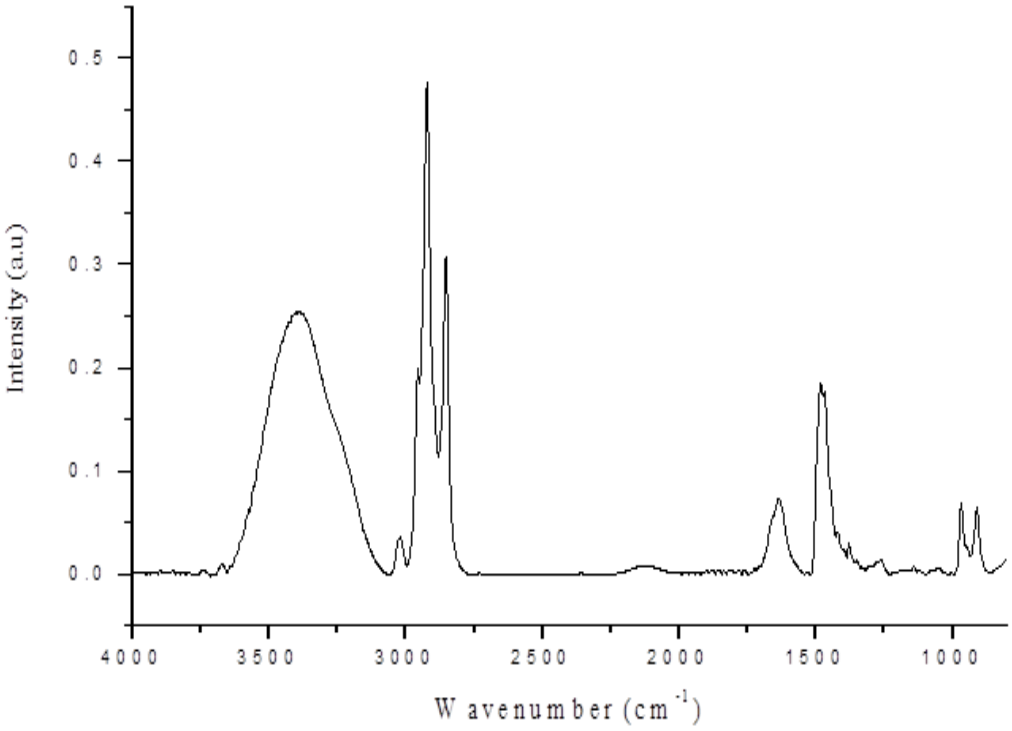

Figure 3-6: IR Spectrum for Surfactant on Mg Alloy AZ31

Figure 3.6 shows the reference infrared spectra for the pure surfactant that was used in this project. The important peaks that indicate the presence of the surfactant molecules in the deposited coating are the CH_2/CH_3 stretch peaks at 2850-3000 cm^{-1}.

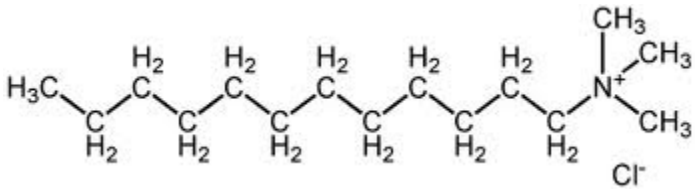

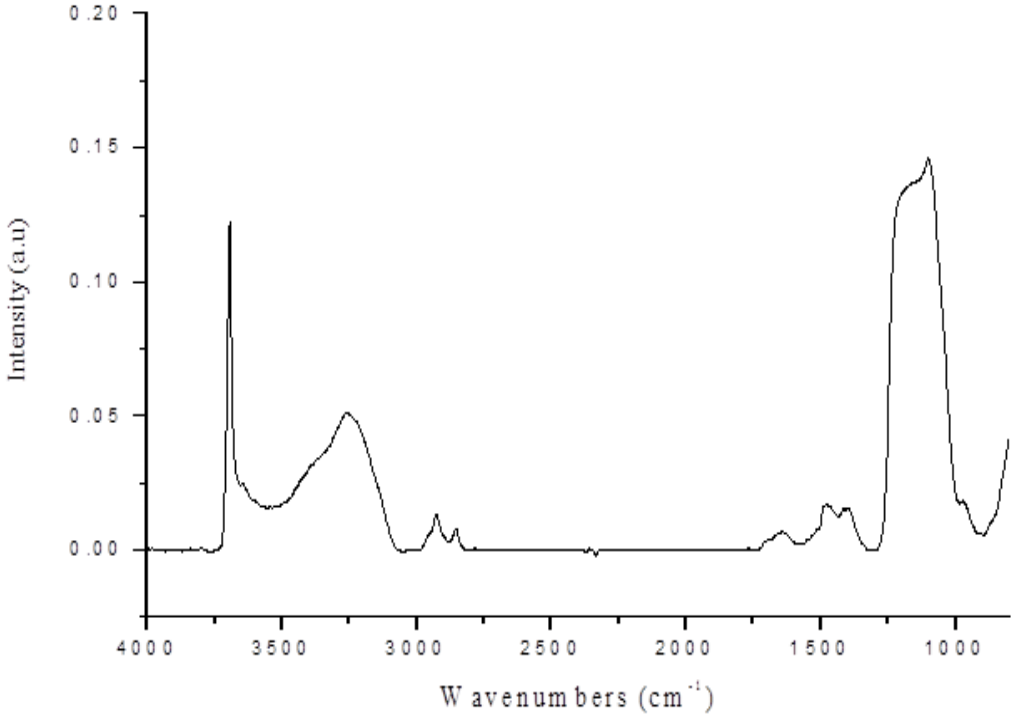

Figure 3-7: IR Spectrum for Particles Layers on Mg Alloy AZ31

A representative infrared spectrum for the as-deposited mesoporous silica layer on bare Mg alloy AZ31 is shown in Figure 3.7. There are three peaks of particular interest that can be attributed to the presence of the mesoporous silica coating on the surface. The first is the (Si-O) peak at 1050-1250 cm^{-1} which indicates the presence of silicate as (Si-O-Si) or (Si-O-Mg). The second is the (CH_2/CH_3) stretch at 2850-3000 cm^{-1} which confirms the presence of the templating agent (surfactant) within the coating. The third is the sharp peak at 3700 cm^{-1} which may be attributed to either Si-OH or Mg-OH.

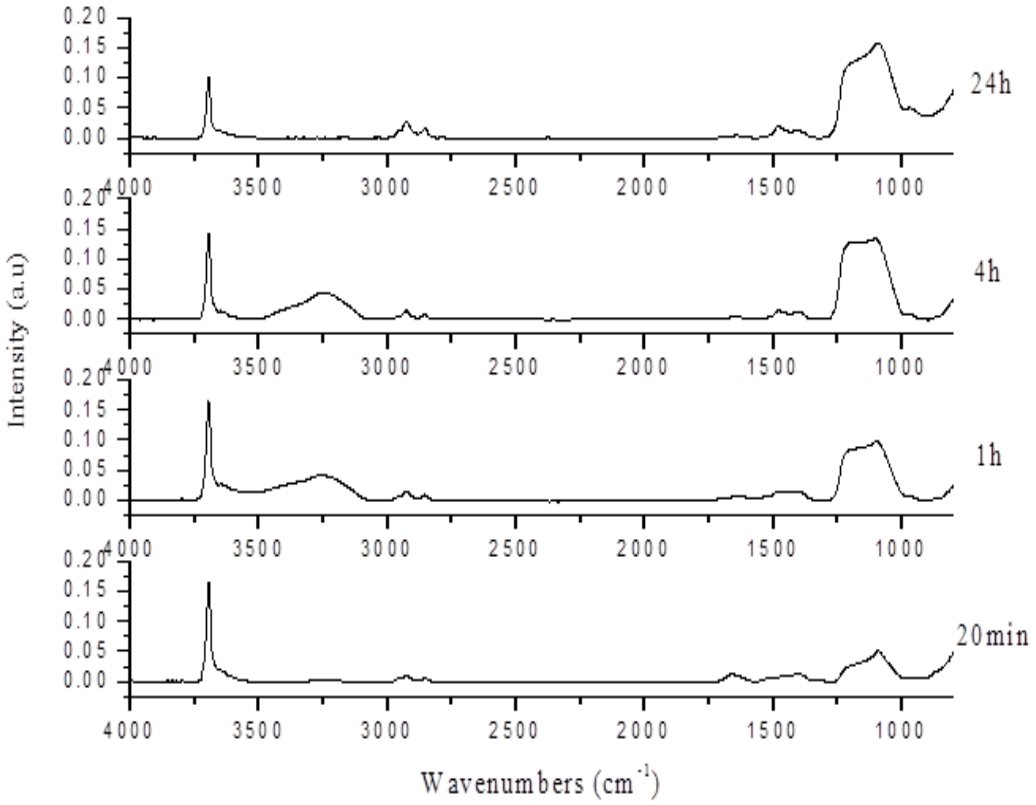

Figure 3-8: IR Spectra of As-Deposited Mesoporous Silica Films at Various Deposition Times

Figure 3.8 shows infrared spectra for magnesium alloys coated with mesoporous silica at various deposition times. All of the peaks that are indicative of the presence of a mesoporous silica film were observed. Unfortunately, it was observed that the Mg alloy began to corrode with increasing deposition time likely due to the presence of the chloride anion of the surfactant in the coating bath. The corrosion was observed when the deposition time was extended to 4 h. Therefore, it was concluded that the best deposition time for the mesoporous silica layer on the Mg alloy was 20 min to 1 h even though the overall thickness of the coating was low as evidenced by the low intensity of the infrared peaks associated with the coating. In order to improve the thickness of the mesoporous silica coating without corrosion of the underlying substrate, multiple treatments/dips in

fresh aliquots of the coating solution was performed. Each successive treatment is designated as a layer in the discussion below.

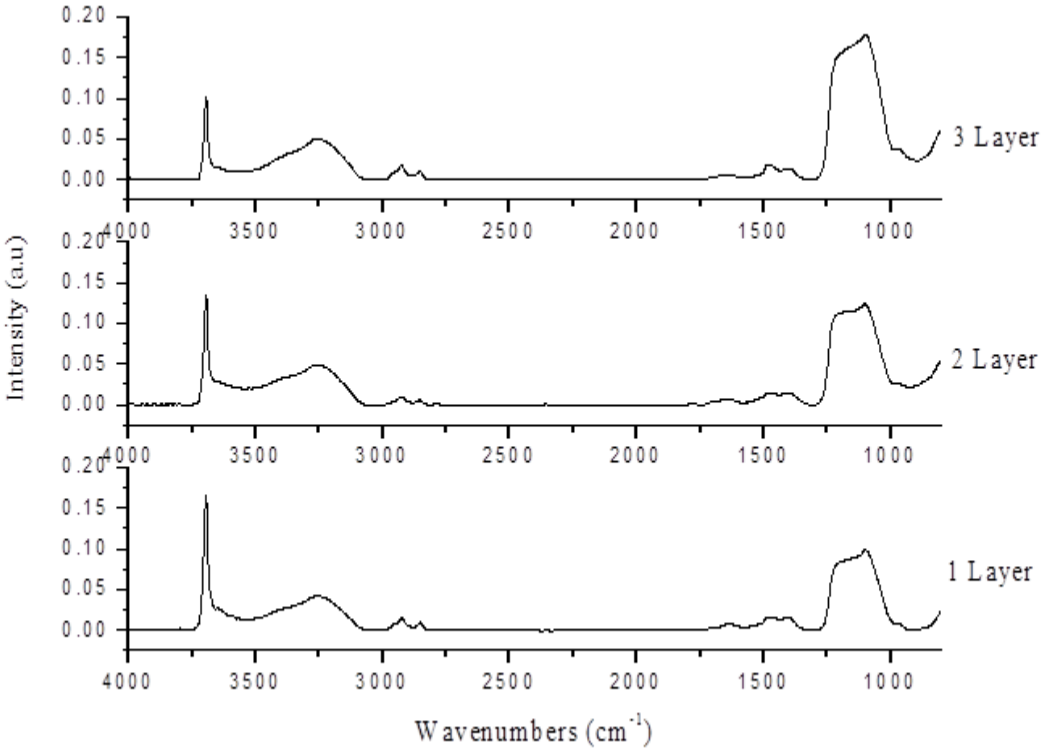

Figure 3-9: IR Spectra for Multiple Mesoporous Silica Treatments

(1h. Deposition Time)

Figure 3.9 shows infrared spectra for samples successively immersed in the mesoporous silica coating solution for three successive 1 h treatments. It is clear that the mesoporous coating is present in all cases and the slight increase in intensity of the Si-O band in these spectra may indicate that the coating thickness increased with an increasing number of treatments. However, it was still observed that the magnesium alloy began to corrode in the coating bath during the third treatment.

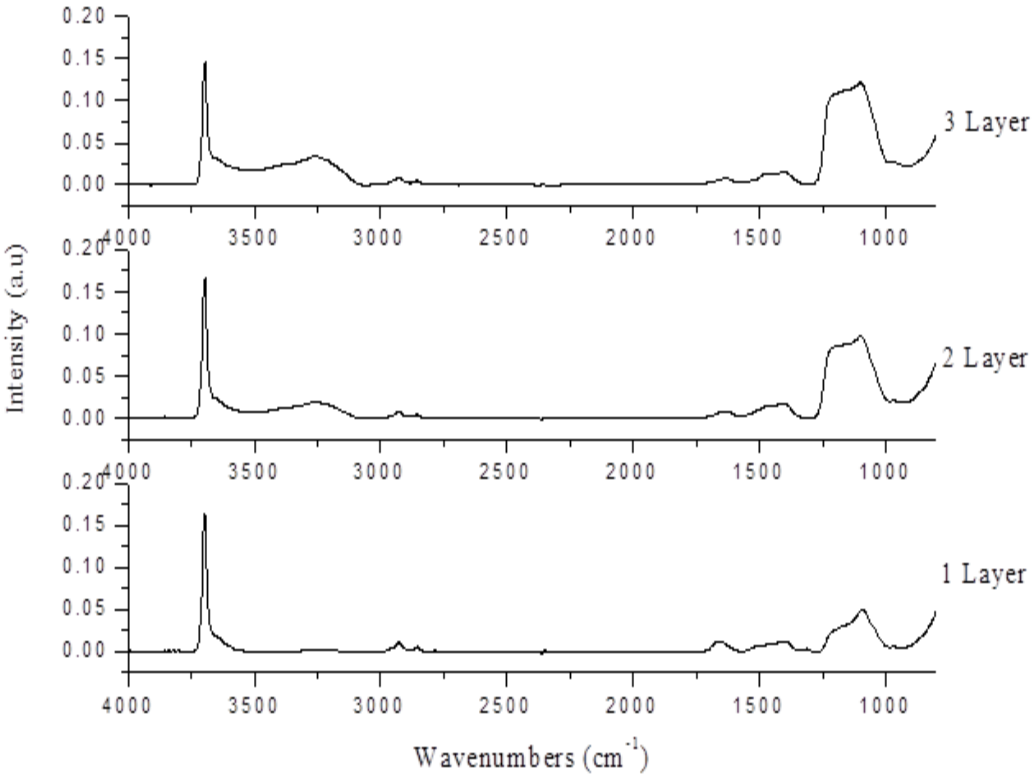

Figure 3-10: IR Spectra for Multiple Mesoporous Silica Treatments

(20 min. Deposition Time)

Figure 3.10 shows infrared spectra for samples successively immersed in the mesoporous silica coating solution for three, 20 minute treatments. No corrosion of the samples in the coating bath was observed even after 3 treatments.

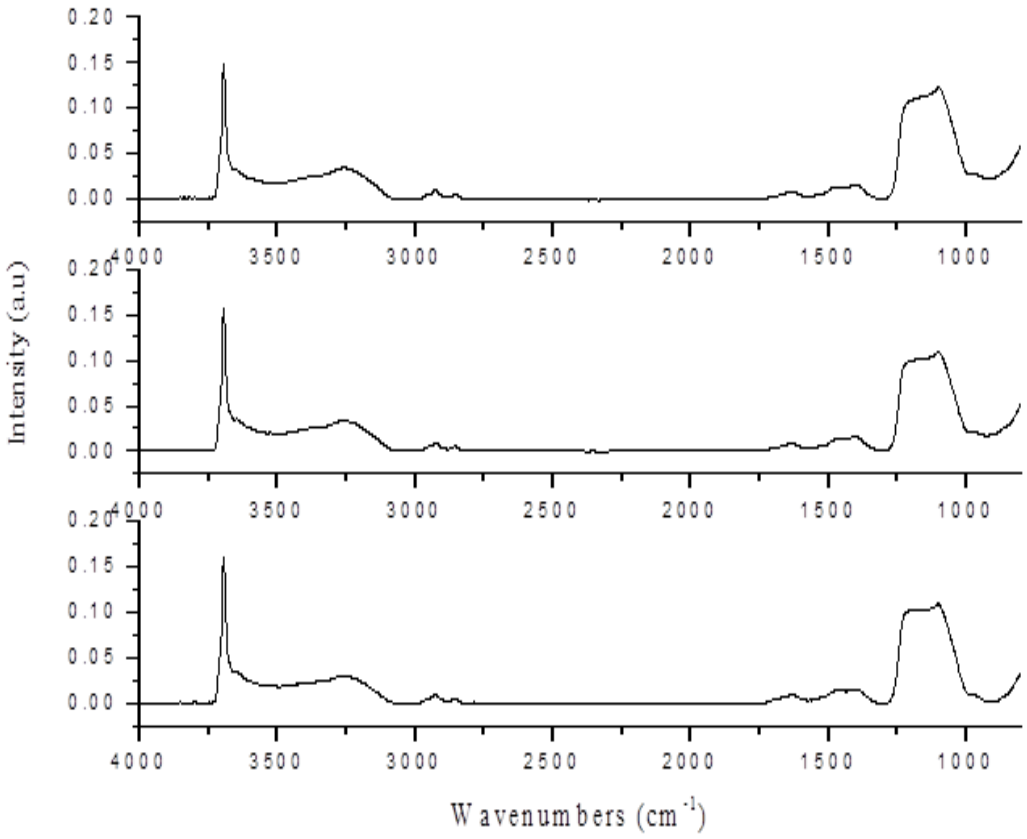

Figure 3-11: IR Spectra for Three Different Spots on an As-Deposited Mesoporous Silica coating as a function of successive treatments/dips in the coating bath. (Deposition time for each layer was 20 min.)

Figure 3.11 shows representative infrared spectra for three different spots on the as-deposited mesoporous silica coating prepared by three treatments/dips for a 20 min. deposition time per layer. Although, these spectra were collected from different spots on the same sample there is no observable difference in the infrared spectra, indicating that the deposited mesoporous silica films are uniformly deposited over the whole surface of the magnesium alloy substrate.

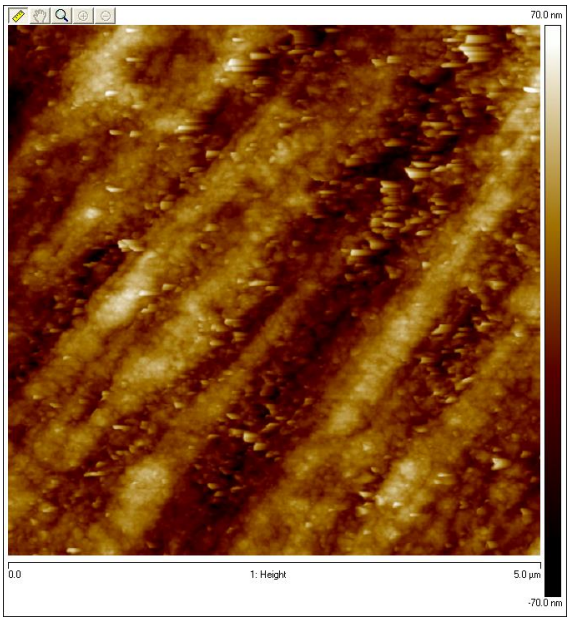

a) AFM image for Mg AZ31 (Control)

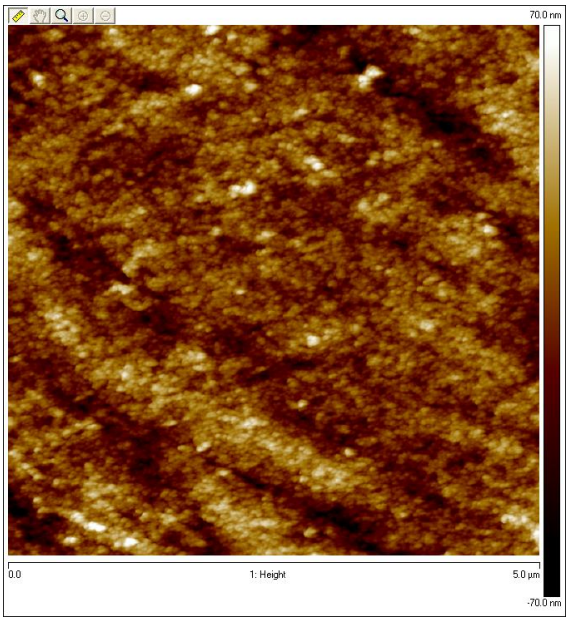

b) AFM image for one particle layer,20 min.

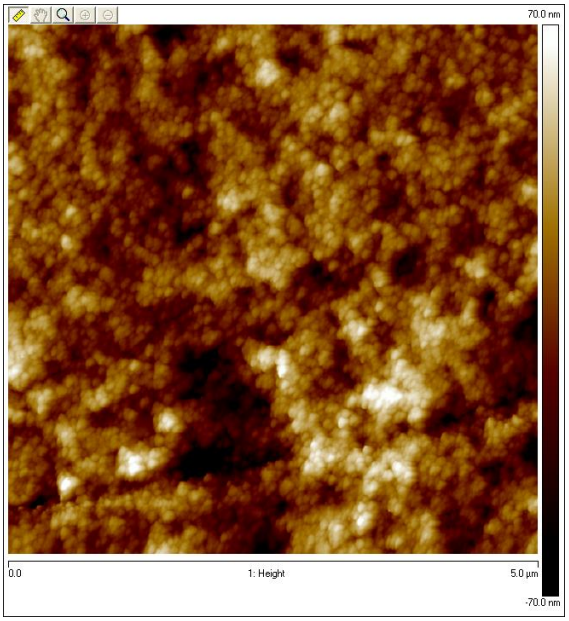

c) AFM image for two particle layer, 20 min

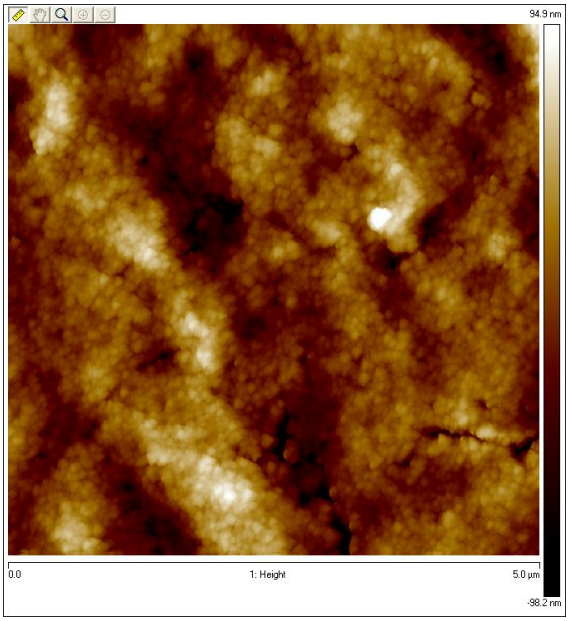

d) AFM image for three particle layer, 20 min

Figure 3-12: 5 µm x 5 µm TM-AFM Images for Magnesium Alloys Coated with as Deposited Mesoporous Silica as a Function Number of Treatments/Layers

Atomic Force Microscopy (AFM) was used to determine the structure of the particles that were deposited on the surface of the magnesium alloy substrate. The images presented are 5 µm x 5 µm. Figure 3.12 shows AFM images for multiple mesoporous silica treatments at a 20 minute deposition time per layer. The uncoated, polished magnesium AZ31 substrate (Figure 3.12a) shows height variations due to the polishing grooves on the surface. Figure 3.12 b shows the magnesium alloy substrate after deposition of a single layer of mesoporous silica. Upon comparison to the unmodified surface, it is clear that the polishing grooves have become less distinct due to the deposition of spherical particles on the surface. The fact that the polishing grooves are still partially visible indicates the formation of a thin layer of the mesoporous silica film on the Mg alloy after the first treatment. This correlates with the observed infrared spectra which show that the intensity of the silica peaks are low after only one layer has been deposited (Figure 3.10). Figure 3.12 c shows the AFM image obtained after the substrate was subjected to a second treatment in the mesoporous coating solution (addition of a second layer). From this image it was observed that after the addition of a second layer of mesoporous silica particles, the polishing grooves of the substrate have completely disappeared and there are many spherical particles on the surface. This indicates that the film thickness increases with the addition of a second layer which correlates with the observed increase in silica peak intensity from the infrared spectrum (Figure 3.10). Finally Figure 3.12 d shows the AFM image of a sample treated with 3 successively deposited layers of mesoporous silica. It is clear from this image that the number of spherical particles increases to the point that a uniform layer of mesoporous silica has deposited on the surface. The increase in the thickness of the layer was again confirmed by the increase in the intensity of the silica bands of the infrared spectra for these samples (Figure 3.10).

The gradual disappearance of the polishing grooves couples with the increase in the number of spherical particles on the surface with the deposition of successive layers indicates that three treatments/layers is sufficient to obtain a uniform film of mesoporous silica particles on the magnesium alloy substrate.

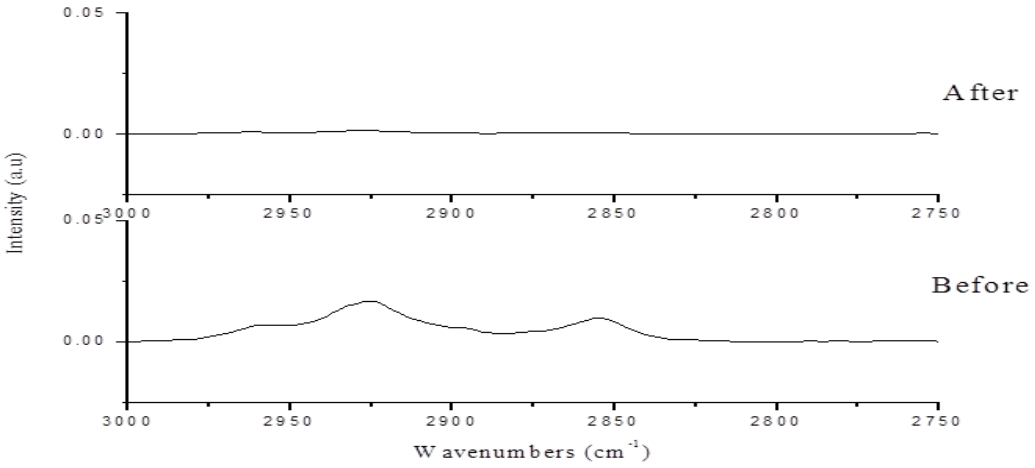

Figure 3-13: IR Spectra for Magnesium Alloys Coated with Multiple Treatments of Mesoporous Silica after and before Calcination

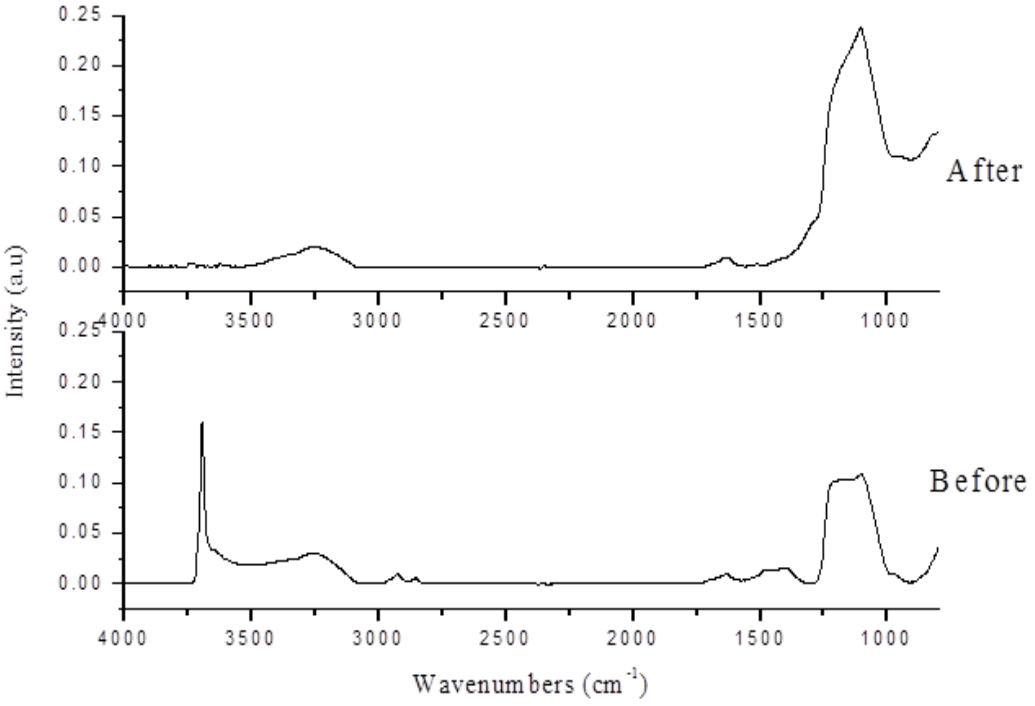

Figure 3-14: IR Spectra for Magnesium Alloys Coated with Multiple Treatments of Mesoporous Silica after and before Calcination

In order to obtain the final mesoporous silica film, the templating agent, in this case a surfactant, must be removed after the coating has been deposited on the surface. Figure 3.13 shows the region of the infrared spectra where the most intense surfactant peaks appear (CH_2/CH_3 stretch, 2850-3000 cm^{-1}) before and after calcination. It was observed that the surfactant peaks disappeared completely after calcination of the coated magnesium substrate.

Figure 3.14 shows the infrared spectra before and after calcination from 800 cm^{-1} to 4000 cm^{-1}. No decrease in intensity of the silica peak (1050-1250 $cm^{-1)}$ was observed indicating that the thermal treatment does not destroy the deposited mesoporous silica film but only removes the surfactant. Moreover, the peak at 3700 cm^{-1} which can be attributed to the presence of either Mg-OH or silanol (Si-OH) peaks has completely disappeared after calcination. If this peak were due to crystalline Mg-OH from the substrate it should have been largely unaffected by thermal treatment. Therefore, this peak has been attributed to Si-OH groups due to incomplete condensation in the mesoporous particles prior to thermal treatment. Thermal treatment leads to the condensation/cross-linking of these silanol groups converting them to silicate Si-O-Si or Si-O-Mg.

3.3 Characterization of the Multi-layered, Bi-Functional Coating (Sol-gel Silica Coating + Mesoporous Silica Film)

The key advantages of depositing a multi-layered, bi-functional coating include an increase of the corrosion resistance of the magnesium alloy by deposition of a sol-gel silica pre-layer followed by a mesoporous silica film to enhance the bioactivity of the magnesium alloy substrate.

The chemistry of the final multi-layered film (sol-gel + mesoporous silica) was confirmed by ATR-FTIR. The properties of the mesoporous silica particles (porosity, surface area) were determined by N_2 adsorption/desorption experiments.

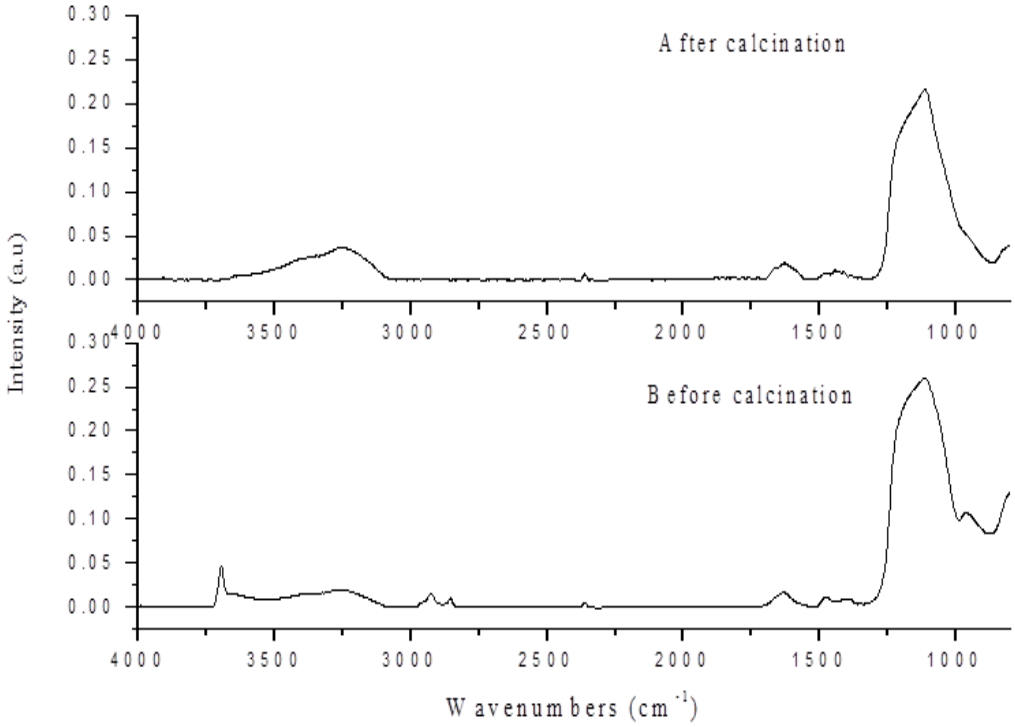

Figure 3-15: IR Spectra for the Final Multi-layered Coating (Sol-gel Silica Coating + Mesoporous Silica Film) before and after Calcination

Figure 3.15 shows infrared spectra for magnesium alloy AZ31 coated with the multi-layered coating (sol-gel silica coating + multiple treatment of mesoporous silica film) before and after calcination. The spectrum for the multi-layered coating before calcination indicates that the final film has all the peaks that are indicative of the presence of a sol-gel silica layer and the as-deposited mesoporous silica film on the surface of magnesium alloy. From the spectra after calcination, it is observed that only the surfactant peaks and the Si-OH bands disappear which demonstrates the formation of the mesoporous structure and the thermal stability of the overall coating.

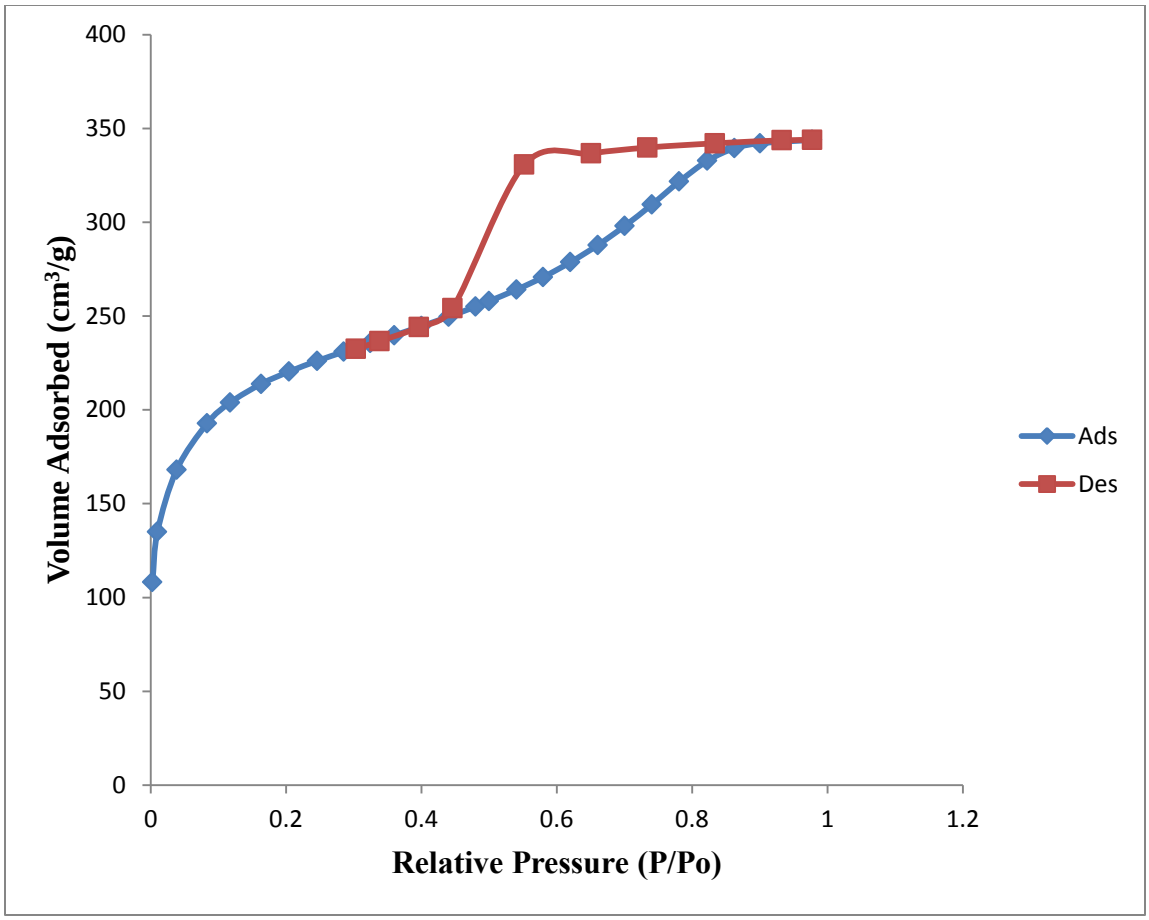

Figure 3-16: N_2 Adsorption/Desorption Isotherms of the Mesoporous Silica Coating

Figure 3.16 shows the N_2 adsorption/desorption isotherms for calcined mesoporous silica powder which was collected from the coating solution. This isotherm can be classified as a type IV isotherm which is characteristic of mesoporous materials according to the IUPAC classification. The isotherm has a large type H_2 hysteresis loop which indicates the presence of mesopores with a variable size distribution. Brunauer-Emmett-Teller (BET) analysis was used to determine the total specific surface area. The BET surface area of the coating is approximately 736 ± 19 m^2/g. From the results obtained by ATR-FTIR and N_2 adsorption/desorption isotherms, it can be concluded that mesoporous silica films with high surface area (due to porosity) were successfully deposited on the magnesium alloy substrate.

3.4 Corrosion Test (FAAS)

In order for implants to be successfully integrated into the human body they must be biocompatible. The use of magnesium and its alloys as a biomaterial is promising due to their good biocompatibility and mechanical properties. However, its degradation rate is too high in the first stages of the healing process. Therefore, it is essential to control the corrosion behaviour of Mg alloys.

This study was to determine the corrosion rate of Mg alloys coated with the final multi-layered coating (sol-gel silica + mesoporous silica film) as well as to identify the corrosion products on the surface. Corrosion tests were done by immersing the coated substrate in simulated body fluid, Hank's balanced salt solution. The mechanism of chemical corrosion reaction in simulated body fluid is described in the introduction (section 1.2.1.1).

FAAS was used to determine the corrosion rate of coated Mg alloys AZ31 in simulated body fluid (SBF) by quantifying the concentration magnesium released into solution as a function of time. As described in section 1.2.1.1, magnesium ions will be released into solution as the magnesium substrate degrades.

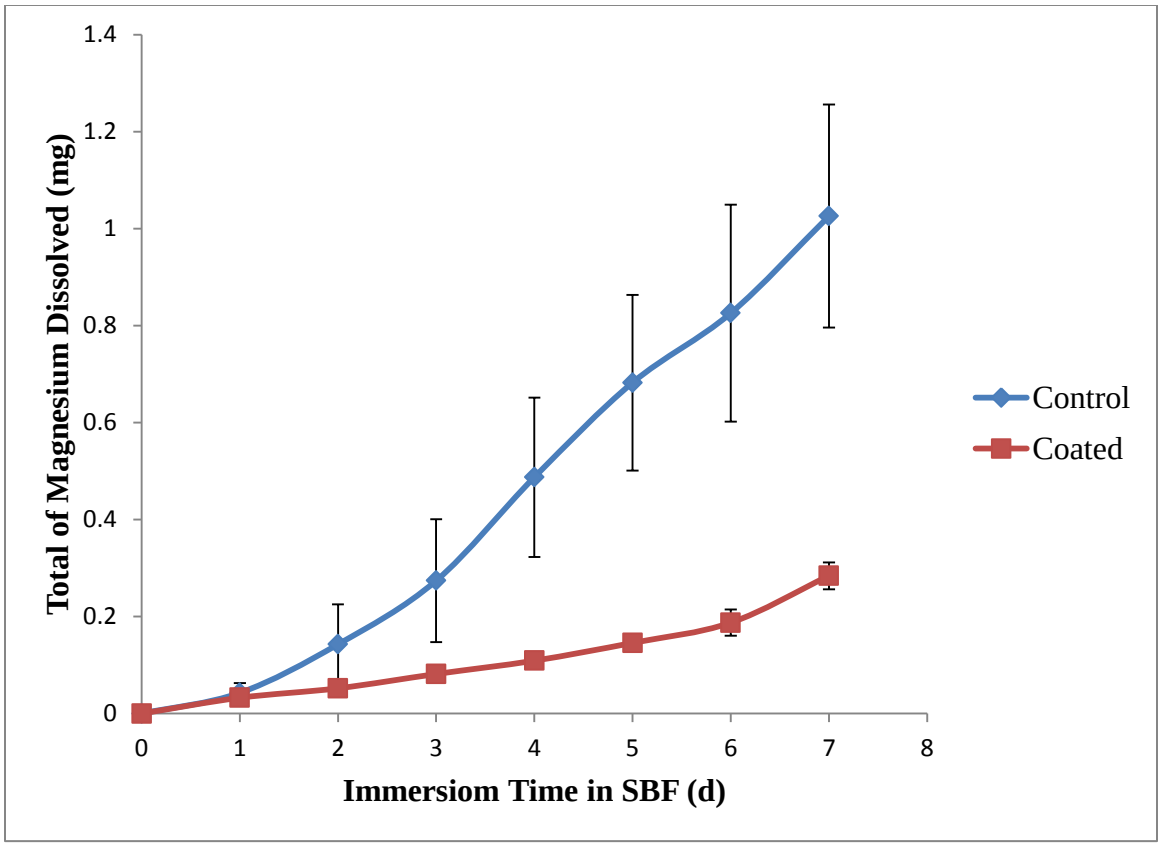

Figure 3-17: Amount of Magnesium Dissolved as a Function of Immersion Time in SBF

Atomic absorption spectroscopy was used to determine the corrosion rate of coated Mg alloys in SBF compared to the uncoated material. Figure 3.17 is a graph of the cumulative amount of magnesium dissolved into the SBF solution as a function of time for a 7 day period. Each data point represents an average of 3 samples; the error bars are the sample to sample standard deviations. Up to day 1, the amount of magnesium released into solution is the same for both samples. However, by day 2 the uncoated material had begun to release magnesium into solution at a high linear rate which continued to the end of the study. By day 7, an average of about 1.03 ± 0.05 mg of magnesium has been released into the SBF solution. In comparison, the release of magnesium into the SBF solution from the coated sample continued in a linear fashion up to 6 days but at a much slower rate than the uncoated sample. At the 7 day mark there appears to be a change in degradation rate of the coated material which may signify that

the coating is beginning to break down. However, the total amount of magnesium released into solution for the coated samples at 7 days is only about 0.284 ± 0.006 mg. This suggests that the uncoated samples degrade at a rate at least 3.5 times greater than the coated samples.

Upon comparison of the coated and uncoated samples, there is a significant difference in the rate of degradation which indicates that the multi-layered coating (sol-gel silica coating + mesoporous silica film) had a strong influence on the corrosion resistance of the magnesium alloy. Longer term studies need to be conducted to determine the corrosion resistance of the coated magnesium alloy compared to a control sample over several months.

3.5 Study on the Bioactivity of the Multi-layered Film:

The formation of hydroxyl apatite on magnesium alloys upon immersion in SBF solution (*in vitro* test) can be a good indication of bioactive behavior *in vivo* and therefore is often used to screen materials for their potential use as bioactive biomaterials. In this study, the bioactivity was evaluated by soaking the coated magnesium alloys in SBF solution (Table 2.3) at 37 °C for different periods of time (1, 3 and 7 days). The ion concentration and pH of SBF solution is similar to that of human blood plasma; this solution contains both calcium and phosphate ions which make it a simple test for the ability of a biomaterial to induce calcium phosphate nucleation and growth at its surface. At each time point, the samples were analyzed by SEM-EDS in order to evaluate the morphology and surface elemental composition of the uncoated and coated magnesium alloy after immersion in SBF. The samples were also analyzed by ATR-FTIR in order to identify the precipitation products on the surface and to determine the stability of the multi-layered film after immersion in SBF.

One of the expected outcomes of the immersion of uncoated magnesium in the SBF solution is the precipitation of calcium phosphate at the surface of the alloy. Calcium phosphates have very low K_{sp} values, especially at elevated pH. As the magnesium alloy degrades, the pH rises resulting in precipitation of calcium phosphate species as shown in

reaction scheme 3.1. Since the SBF is supersaturated with calcium and phosphate, this reaction readily occurs during immersion in the SBF environment. It could therefore be argued that magnesium based implant materials are inherently bioactive. However, the calcium phosphate coatings that deposit on the surface via this mechanism are typically non-uniform, non-adherent precipitation products that do not impart sufficient corrosion resistance to the material.

Reaction Scheme 3.1: Precipitation Reactions.

$$10Ca^{2+}_{(aq)} + 6PO_4^{3-}{}_{(aq)} + 2OH^-_{(aq)} \rightarrow Ca_{10}(PO_4)_6(OH)_{2(s)}$$

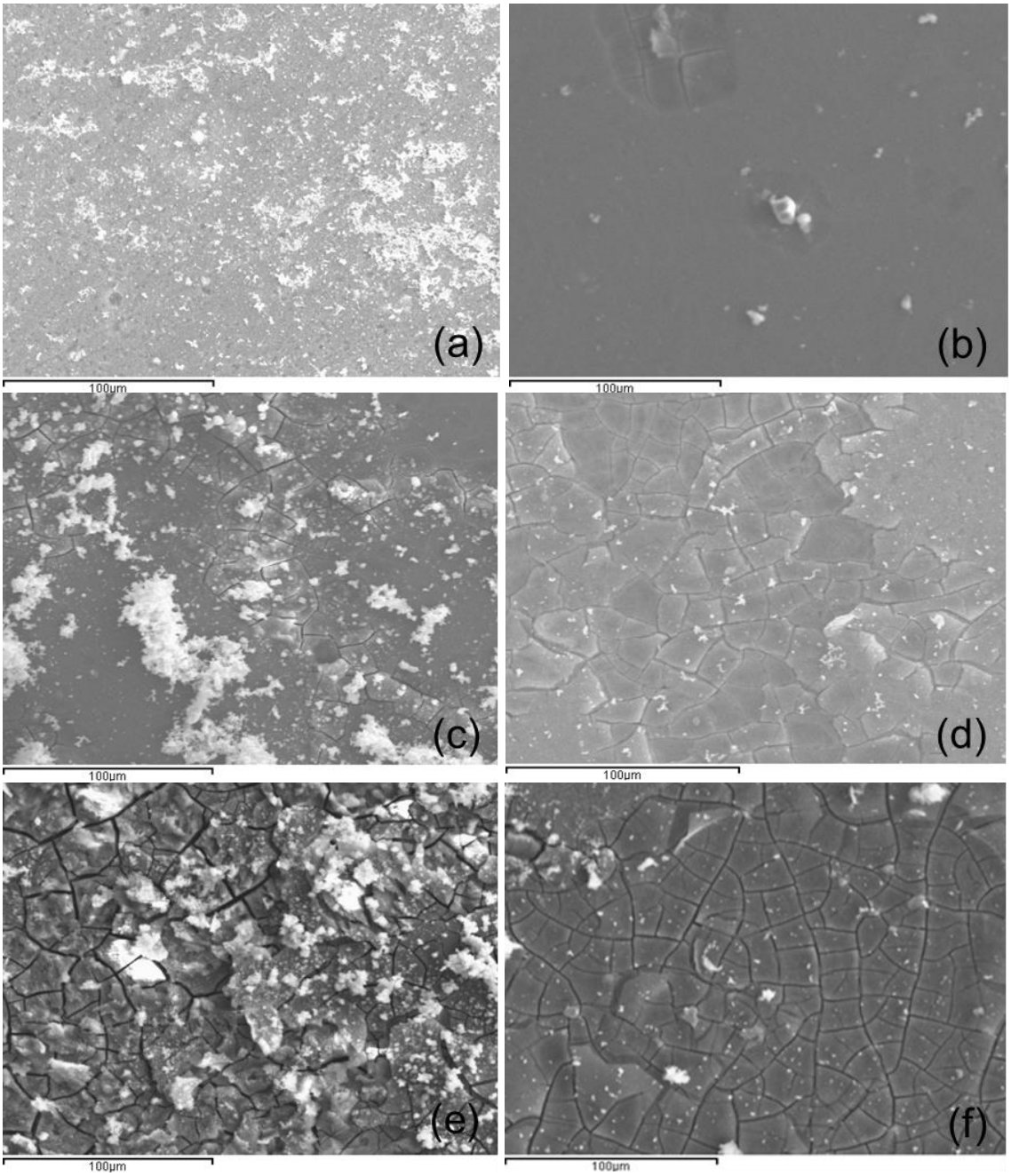

Figure 3-18: SEM Images of Coated and Uncoated Mg AZ31 Alloys after Immersion in SBF for Different of Time; (a) Uncoated (b) Coated Sample after 1 Day Immersion, (c) Uncoated (d) Coated after 3 Days Immersion, (e) Uncoated (f) Coated after 7 Days Immersion

Figure 3.18 shows SEM images of the coated and uncoated magnesium alloys after immersion in SBF for different times. It is observed from SEM images (a-c-e) that the uncoated sample is completely covered with calcium phosphate layer after immersion in SBF for seven days which was expected due to its high corrosion rate which induces precipitation of calcium phosphate at the interface. Pitting and cracks are readily observed on the magnesium substrate after 1 day and 3 days immersion in SBF. Furthermore, non-uniformly distributed calcium phosphate clusters were observed on the surface of these samples. After a 7 day immersion in the SBF solution, the surface of the uncoated magnesium alloy was completely covered with a thick layer of calcium phosphate. The presence of both calcium and phosphorus on these samples surfaces was confirmed by EDS and will be discussed in more detail in subsequent sections.

In contrast, the SEM images (b-d-f) for the coated sample after immersion in SBF, are still smooth after immersion in SBF for one day with the exception of a few small calcium phosphate clusters randomly distributed across the surface. After three days of immersion in SBF, a uniform layer of calcium phosphate is observed on the surface which increases in thickness with increasing immersion time (7 days, Figure 3.18 f). In comparison to the uncoated sample this calcium phosphate layer is thin and uniform.

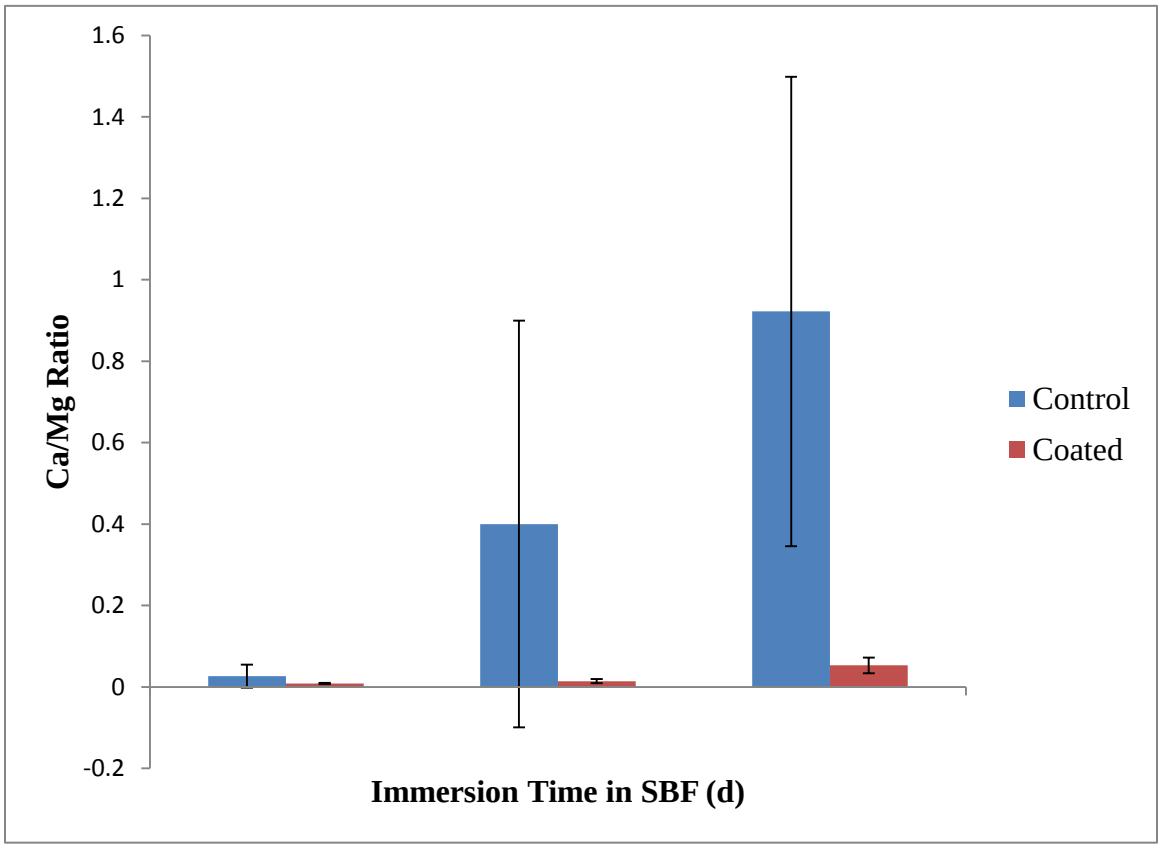

Figure 3-19: The Ratio of Calcium/Magnesium after Immersion the Coated and Uncoated (Control) Samples in SBF for Different Times

All the samples were analyzed by EDS for evaluation of elemental composition of the new formed bioactive layer on the surface of the coated and uncoated samples.

Figure 3.19 shows the ratio of Ca/Mg after immersion in SBF as a function of immersion time. The EDS analysis suggests that the ratio of calcium/magnesium on the uncoated sample surface increases with increasing immersion time in SBF. In comparison, the ratio of calcium/magnesium on the coated sample surface is constant for the first three days of immersion in SBF and then increases significantly after 7 days indicating an increase in the thickness of the calcium phosphate layer with increasing immersion time.

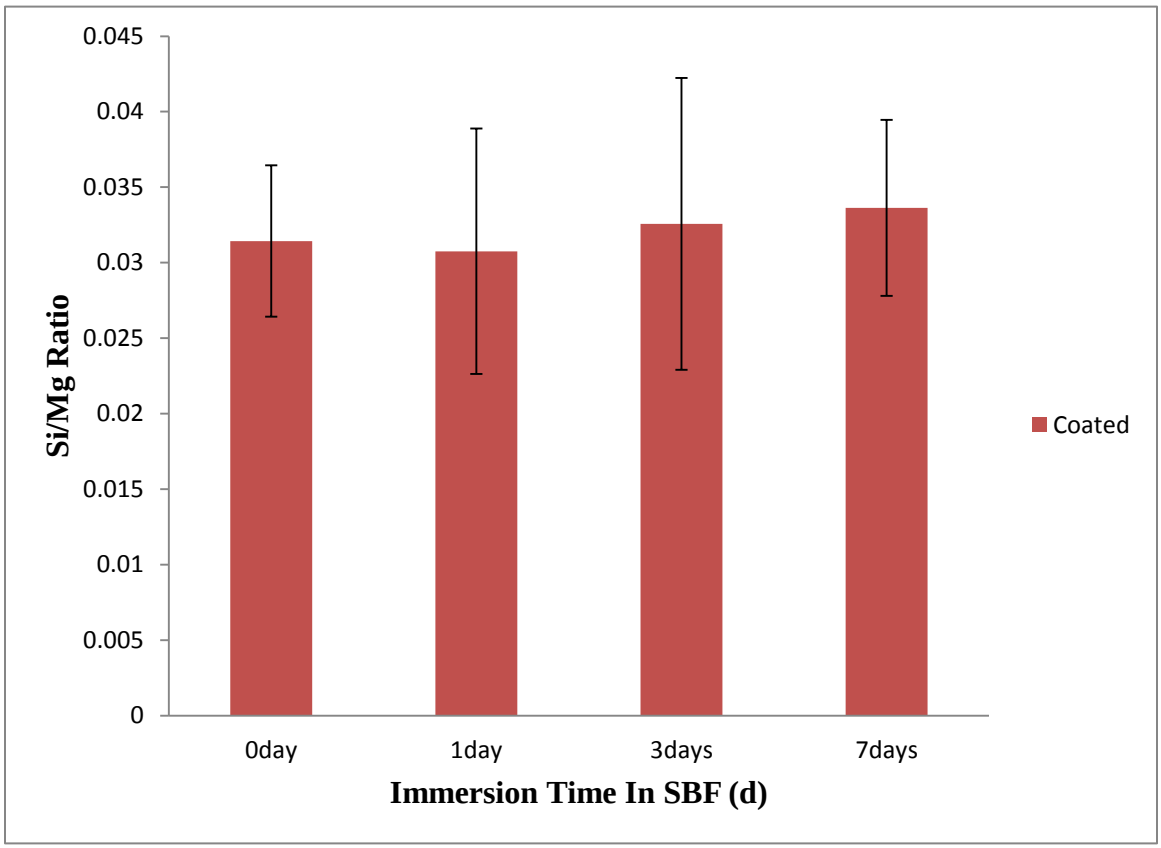

Figure 3-20: The Ratio of Silicon/Magnesium after Immersion the Coated Samples in SBF for Different Times

Figure 3.20 shows the ratio of silicon/magnesium after immersion of the coated samples in SBF for different times. The average ratios of silicon/magnesium on the coated sample are still constant even after a 7 day immersion in SBF. This suggests the multi-layered coating has likely not degraded.

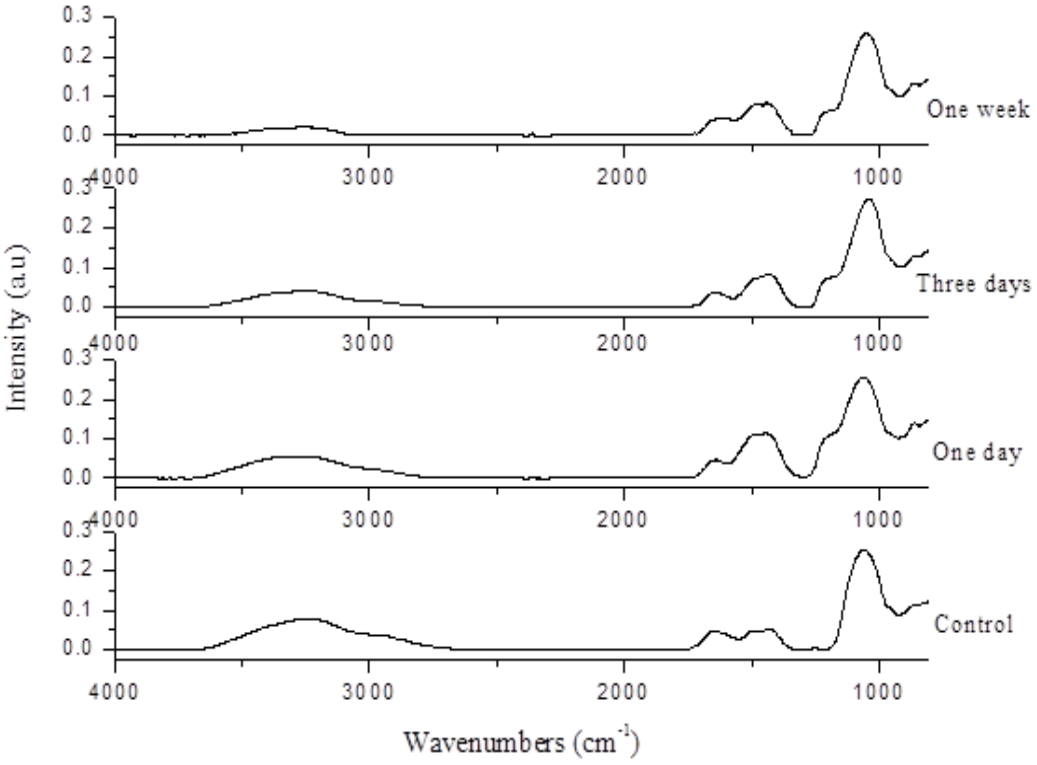

Figure 3-21: IR Spectra for the Final Multi-layered Coating after Immersion in SBF for Various Periods of Time

Figure 3.21 shows infrared spectra for magnesium alloys coated with the final multi-layered coating and immersed in SBF for 1, 3 and 7 days. As shown in this figure, both the uncoated and coated samples have a strong phosphate peak at 1050 cm^{-1} confirming that the phosphorus peak observed in the EDS spectra is due to the presence of phosphate at the surface (Table 3.1). The coated samples also have a distinct peak due to silica that appears as a shoulder at 1200 cm^{-1}. This indicates that the multi-layered coating remains intact even after 7 days of exposure to SBF.

Table 3-1: The Atomic Percentages of Mg-Si-P-Ca after Immersion the Coated and Uncoated (Control) Samples in SBF for Different Times

Immersion Time in SBF (Day)	Sample	Magnesium (Mg)	Silicon (Si)	Phosphorous (P)	Calcium (Ca)
1	Control	59.5 ±30.4	_	2.2±0.3	1.0±0.4
	Coated	66.1±9.1	2±0.5	1.3±0.1	0.5±0.1
3	Control	45.2±30.2	_	10.1±9.2	8.2±8.3
	Coated	56.8±9.5	1.8±0.5	2.0±0.5	0.8±0.2
7	Control	11.7±3.5	_	8.7±2.3	9.2±3.4
	Coated	41.5±5.1	1.4±0.3	5.4±1.2	2.2±0.7

The SEM-EDS results coupled with the infrared analysis shown above suggests that the coating protects the surface of the magnesium alloy from corrosion in SBF resulting in a change in mechanism for calcium phosphate deposition on the coated vs. uncoated substrate. On the uncoated substrate, nucleation and growth of the calcium phosphate is predominantly due to a rise in pH at the interface resulting in the precipitation of calcium phosphate as a corrosion product. On the coated samples the corrosion is minimized and nucleation and growth of calcium phosphate may result from local high concentrations of calcium and phosphate ions within the pores of the mesoporous silica coating. Further studies are needed to confirm this deposition mechanism. However, it is clear from these results that the coated magnesium alloy is stable in SBF and bioactive; the deposition of calcium phosphate was observed within 1 day of immersion in the SBF solution.

Chapter 4

4 « Conclusions and Future Direction »

From the results obtained by ATR-FTIR, AFM and N_2 adsorption/desorption isotherms, it can be concluded that multi-layered coatings were successfully deposited on magnesium alloy AZ31 by using silane as a protective pre-layer and mesoporous silica as a bioactive coating. The optimum conditions for deposition of the sol-gel silica protective pre-layer on Mg alloy were determined to be a high concentration of TEOS (3.2% v/v) with a short deposition time (20 min). Furthermore, the optimum mesoporous silica coating was obtained by multiple treatments in the coating bath at short deposition times to produce multi-layered mesoporous silica film with good uniformity and a high surface area.

The final multi-layered coating (sol-gel silica coating + mesoporous silica film) was shown to induce the formation of a calcium phosphate layer on the coated surface in SBF indicating its potential as a bioactive coating. In addition, this coating was also observed to significantly enhance the corrosion resistance of the magnesium alloy in SBF.

While these results show that multi-layered, bi-functional coatings can enhance the corrosion resistance of magnesium alloys while maintaining their bioactivity further research is needed to better understand the mechanism of bioactivity of these coatings. Furthermore, *in vitro* degradation studies to determine the corrosion resistance of these coating over longer immersion times in SBF are needed. As well, the behaviour of these silica coatings on magnesium alloys *in vivo* has not been studied. This issue will need to be addressed prior to the implementation of these coating in a clinical setting. Finally, the possibility of using this mesoporous silica coating as a local drug delivery system should be investigated. The potential to load the pores with anti-inflammatory drugs, antibacterial agents and possibly growth factors could provide a route to significantly improve the overall biocompatibility of magnesium alloy based implant materials.

5 References

1. Leali, P. T., and Merolli, A. "Fundamentals of Biomaterials." *Biomaterials in Hand Surgery*. Milan: Springer (2009): 1-11.

2. Ratner, B. D., Hoffman, A. S., Schoen, F. J., and Lemons, J. E. "Biomaterials science." *Plasma processing of polymers*. Netherlands: Kluwer Academic Publisher (1997): 453-464.

3. Parida, P., Behera, A., and Mishra, S. C. "Classification of Biomaterials used in Medicine." *International Journal of Advances in Applied Sciences* 1.3 (2012): 31-35.

4. Malekani, J., Schmutz, B., Gu, Y., Schuetz, M., and Yarlagadda, P. K. "Biomaterials in orthopedic bone plates: a review." *Proceedings of the 2nd Annual International Conference on Materials Science, Metal & Manufacturing (M3 2011)*. Global Science and Technology Forum (2011): 71-77.

5. Gonzalez, F. A. "Introduction to Biomaterials in Orthopaedic Surgery." *Biomaterials in orthopaedic surgery*. Materials Park, Ohio: ASM International (2009): 1-9.

6. Heness, G., and Ben-Nissan, B. "Innovative bioceramics." *Materials forum* 27.0 (2004): 104 -114.

7. Hermawan, H. "Biodegradable Metals: State of the Art." *Biodegradable Metals*. Berlin: Springer (2012): 13-22.

8. Staiger, M. P., Pietak, A. M., Huadmai, J., and Dias, G. "Magnesium and its alloys as orthopedic biomaterials: a review." *Biomaterials* 27.9 (2006): 1728-1734.

9. Yang, J. X., Cui, F. Z., Lee, I. S., Zhang, Y., Yin, Q. S., Xia, H., and Yang, S. X. "In vivo biocompatibility and degradation behavior of Mg alloy coated by

calcium phosphate in a rabbit model." *Journal of Biomaterials Applications* 27.2 (2012): 153-164.

10. Bogden, J. D., and M. Klevay, L. *Clinical nutrition of the essential trace elements and minerals: the guide for health professionals*. New Jersey: Humana Press (2000).

11. Gupta, M., and Sharon, M.N.L. *Magnesium, magnesium alloys, and magnesium composites*. Hoboken, New Jersey: Wiley (2011).

12. Okuma, T. "Magnesium and bone strength." *Nutrition* 17.7 (2001): 679-680.

13. Qin, L. *Advanced bioimaging technologies in assessment of the quality of bone and scaffold materials: Techniques and applications*. Berlin: Springer Verlag (2007).

14. Swaminathan, R. "Magnesium metabolism and its disorders." *The Clinical Biochemist Reviews* 24.2 (2003): 47.

15. Gray-Munro, J. E., Seguin, C., and Strong, M. "Influence of surface modification on the in vitro corrosion rate of magnesium alloy AZ31." *Journal of Biomedical Materials Research Part A* 91.1 (2009): 221-230.

16. Rosalbino, F., De Negri, S., Saccone, A., Angelini, E., and Delfino, S. "Bio-corrosion characterization of Mg–Zn–X (X= Ca, Mn, Si) alloys for biomedical applications." *Journal of Materials Science: Materials in Medicine* 21.4 (2010): 1091-1098.

17. Carboneras, M., García-Alonso, M. C., and Escudero, M. L. "Biodegradation kinetics of modified magnesium-based materials in cell culture medium." *Corrosion Science* 53.4 (2011): 1433-1439.

18. Xu, R., Wu, G., Yang, X., Hu, T., Lu, Q., and Chu, P. K. "Controllable degradation of biomedical magnesium by chromium and oxygen dual ion implantation." *Materials Letters* 65.14 (2011): 2171-2173.

19. Zeng, R., Dietzel, W., Witte, F., Hort, N., and Blawert, C. "Progress and challenge for magnesium alloys as biomaterials." *Advanced Engineering Materials* 10.8 (2008): B3-B14.

20. Shaw, B.A. Corrosion resistance of magnesium alloys: Handbook. *ASM International* 13A (2003): 692-696.

21. Song, G. "Control of biodegradation of biocompatable magnesium alloys." *Corrosion Science* 49.4 (2007): 1696-1701.

22. Schuh, G. "Fiber-Reinforced Plastics Enable New Prospects." *Future trends in production engineering proceedings of the first Conference of the German Academic Society for Production Engineering (WGP)*, Berlin: Springer, 2013. 299-331.

23. Bakhsheshi-Rad, H. R., Idris, M. H., Abdul-Kadir, M. R., Ourdjini, A., Medraj, M., Daroonparvar, M., and Hamzah, E. "Mechanical and bio-corrosion properties of quaternary Mg–Ca–Mn–Zn alloys compared with binary Mg–Ca alloys." *Materials & Design* 53 (2014): 283-292.

24. Gu, X. N., and Zheng, Y.F. "A review on magnesium alloys as biodegradable materials." *Frontiers of Materials Science in China* 4.2 (2010): 111-115.

25. Scott, A. F., Gray-Munro, J. E., and Shepherd, J. L. "Influence of coating bath chemistry on the deposition of 3-mercaptopropyl trimethoxysilane films deposited on magnesium alloy." *Journal of colloid and interface science* 343.2 (2010): 474-483.

26. Ambat, R., Aung, N. N., and Zhou, W.. "Evaluation of microstructural effects on corrosion behaviour of AZ91D magnesium alloy." *Corrosion science* 42.8 (2000): 1433-1455.

27. Ambat, R., Aung, N. N., and Zhou, W. "Corrosion resistance of magnesium alloy (AZ31E) as orthopaedic biomaterials in sodium chloride containing antioxidantly

active compounds from Eichhornia crassipes." *Int J Electrochem Sci* 6 (2011): 3017-3035.

28. Song, G., and A. Atrens. "Recent insights into the mechanism of magnesium corrosion and research suggestions." Advanced Engineering Materials 9.3 (2007): 177-183.

29. Makar, G. L., and Kruger, J. "Corrosion of magnesium." *International Materials Reviews* 38.3 (1993): 138-153.

30. Wang, Y., Wei, M., Gao, J., Hu, J., and Zhang, Y. "Corrosion process of pure magnesium in simulated body fluid." *Materials letters* 62.14 (2008): 2181-2184.

31. Gray, J. E., and Luan, B. "Protective coatings on magnesium and its alloys—a critical review." *Journal of alloys and compounds* 336.1 (2002): 88-113.

32. Pardo, A., Merino, M. C., Coy, A. E., Arrabal, R., Viejo, F., and Matykina, E. "Corrosion behaviour of magnesium/aluminium alloys in 3.5 wt.% NaCl." *Corrosion Science* 50.3 (2008): 823-834.

33. Zhou, X., Huang, Y., Wei, Z., Chen, Q., and Gan, F. "Improvement of corrosion resistance of AZ91D magnesium alloy by holmium addition." *Corrosion Science* 48.12 (2006): 4223-4233.

34. Gomez-Vega, J. M., Hozumi, A., Saiz, E., Tomsia, A. P., Sugimura, H., and Takai, O. "Bioactive glass–mesoporous silica coatings on Ti6Al4V through enameling and triblock-copolymer-templated sol-gel processing." *Journal of biomedical materials research* 56.3 (2001): 382-389.

35. Khramov, A. N., Balbyshev, V. N., Kasten, L. S., and Mantz, R. A. "Sol–gel coatings with phosphonate functionalities for surface modification of magnesium alloys." *Thin Solid Films* 514.1 (2006): 174-181.

36. Thim, G. P., Oliveira, M. A., Oliveira, E. D., and Melo, F. C. "Sol–gel silica film preparation from aqueous solutions for corrosion protection." *Journal of non-crystalline solids* 273.1 (2000): 124-128.

37. Wang, Duhua, and Bierwagen, G. P. "Sol–gel coatings on metals for corrosion protection." *Progress in organic coatings* 64.4 (2009): 327-338.

38. Pierre, A. C., and Pajonk, G. M. "Chemistry of aerogels and their applications." *Chemical Reviews* 102.11 (2002): 4243-4266.

39. Hong, J. U., Kumar, A. K., Han, H. S., Koo, Y. H., Kim, H. W., Park, J. H., Kang, H.S., Lee, B. C., Piao, L., and Kim, S. H. "Alkoxysilane Adhesion Promoter for Ag Nano-Ink." *Notes* 34.8 (2013): 2539.

40. Supplit, R., Koch, T., and Schubert, U. "Evaluation of the anti-corrosive effect of acid pickling and sol–gel coating on magnesium AZ31 alloy." *Corrosion Science* 49.7 (2007): 3015-3023.

41. Supplit, R., and Schubert, U. "Corrosion protection of aluminum pigments by sol–gel coatings." *Corrosion science* 49.8 (2007): 3325-3332.

42. Metroke, T. L., Parkhill, R. L., and Knobbe, E. T. "Passivation of metal alloys using sol–gel-derived materials—a review." *Progress in Organic Coatings* 41.4 (2001): 233-238.

43. Brinker, C. J., and Scherer, G.W. *Sol-gel science.: the physics and chemistry of sol-gel processing*. Boston: Academic Press, 1990.

44. Hench, L. L., and West, J.K. "The sol-gel process." *Chemical Reviews* 90.1 (1990): 33-72.

45. Matinlinna, J. P., et al. "An introduction to silanes and their clinical applications in dentistry." *The International journal of prosthodontics* 17.2 (2003): 155-164.

46. Vasconcelos, D. C. L., Carvalho, J. A. N., Mantel, M., and Vasconcelos, W. L. "Corrosion resistance of stainless steel coated with sol–gel silica." *Journal of Non-Crystalline Solids* 273.1 (2000): 135-139.

47. Galliano, P., De Damborenea, J. J., Pascual, M. J., and Durán, A. "Sol-gel coatings on 316L steel for clinical applications." *Journal of sol-gel science and technology* 13.1-3 (1998): 723-727.

48. Naik, B., and Ghosh, N. N. "A review on chemical methodologies for preparation of mesoporous silica and alumina based materials." *Recent patents on nanotechnology* 3.3 (2009): 213-224.

49. Athens, G. L., Shayib, R. M., and Chmelka, B. F. "Functionalization of mesostructured inorganic–organic and porous inorganic materials." *Current Opinion in Colloid & Interface Science* 14.4 (2009): 281-292.

50. Suteewong, T., Sai, H., Bradbury, M., Estroff, L. A., Gruner, S. M., & Wiesner, U. "Synthesis and Formation Mechanism of Aminated Mesoporous Silica Nanoparticles." *Chemistry of Materials* 24.20 (2012): 3895-3905.

51. Tang, F., Li, L., and Chen, D. "Mesoporous silica nanoparticles: synthesis, biocompatibility and drug delivery." *Advanced Materials* 24.12 (2012): 1504-1534.

52. Asefa, T., and Tao, Z. "Mesoporous silica and organosilica materials-Review of their synthesis and organic functionalization." *Canadian Journal of Chemistry* 90.12 (2012): 1015-1031.

53. Boissière, C., Larbot, A., and Prouzet, E. "Synthesis of mesoporous MSU-X materials using inexpensive silica sources." *Chemistry of materials* 12.7 (2000): 1937-1940.

54. Jo, C., Kim, K., and Ryoo, R. "Syntheses of high quality KIT-6 and SBA-15 mesoporous silicas using low-cost water glass, through rapid quenching of silicate

structure in acidic solution." *Microporous and Mesoporous Materials* 124.1 (2009): 45-51.

55. Asefa, T., and Tao, Z. "Biocompatibility of mesoporous silica nanoparticles." *Chemical Research in Toxicology* 25.11 (2012): 2265-2284.

56. Izquierdo-Barba, I., Ruiz-González, L., Doadrio, J. C., González-Calbet, J. M., and Vallet-Regí, M. "Tissue regeneration: a new property of mesoporous materials." *Solid state sciences* 7.8 (2005): 983-989.

57. Smarsly, B., Polarz, S., and Antonietti, M. "Preparation of porous silica materials via sol-gel nanocasting of nonionic surfactants: A mechanistic study on the self-aggregation of amphiphiles for the precise prediction of the mesopore size." *The Journal of Physical Chemistry B* 105.43 (2001): 10473-10483.

58. Schramm, L.L, Stasiuk, E. N., and Marangoni, D. G. "Surfactants and their applications." *Annual Reports Section "C" (Physical Chemistry)* 99. (2003): 3-48.

59. Chen, J., Zhang, R., Han, L., Tu, B., and Zhao, D. "One-pot synthesis of thermally stable gold@ mesoporous silica core-shell nanospheres with catalytic activity." *Nano Research* 6.12 (2013): 871-879.

60. Lin, H. P., and Mou, C.Y. "Salt effect in post-synthesis hydrothermal treatment of MCM-41." *Microporous and mesoporous materials* 55.1 (2002): 69-80.

61. Puanngam, M., and Unob, F. "Preparation and use of chemically modified MCM-41 and silica gel as selective adsorbents for Hg (II) ions." *Journal of hazardous materials* 154.1 (2008): 578-587.

62. Giraldo, L. F., Lopez, B. L., Perez, L., Urrego, S., Sierra, L., and Mesa, M. "Mesoporous silica applications." *Macromolecular symposia* 258.1 (2007): 129-141.

63. Giraldo, L. F., Lopez, B. L., Perez, L., Urrego, S., Sierra, L., and Mesa, M. "Mesoporous silica nanoparticles for drug delivery and biosensing applications." *Advanced Functional Materials* 17.8 (2007): 1225-1236.

64. Izquierdo-Barba, I., Colilla, M., and Vallet-Regí, M. "Nanostructured mesoporous silicas for bone tissue regeneration." *Journal of Nanomaterials* 2008 (2008): 60.

65. Lu, J., Liong, M., Zink, J. I., and Tamanoi, F. "Mesoporous silica nanoparticles as a delivery system for hydrophobic anticancer drugs." *Small* 3.8 (2007): 1341-1346.

66. Zhou, H., Wu, X., Wei, J., Lu, X., Zhang, S., Shi, J., and Liu, C. "Stimulated osteoblastic proliferation by mesoporous silica xerogel with high specific surface area." *Journal of Materials Science: Materials in Medicine* 22.3 (2011): 731-739.

67. Lozano, D., Manzano, M., Doadrio, J. C., Salinas, A. J., Vallet-Regí, M., Gómez-Barrena, E., and Esbrit, P. "Osteostatin-loaded bioceramics stimulate osteoblastic growth and differentiation." *Acta biomaterialia* 6.3 (2010): 797-803.

68. Katiyar, A., Ji, L., Smirniotis, P. G., and Pinto, N. G. "Adsorption of bovine serum albumin and lysozyme on siliceous MCM-41." *Microporous and mesoporous materials* 80.1 (2005): 311-320.

69. Vallet-Regí, M., Garcia, M. M., and Colilla, M. "*Biomedical Applications of Mesoporous Ceramics: Drug Delivery, Smart Materials, and Bone Tissue Engineering.*" Boca Raton, FL: CRC Press, 2012.

70. Pang, J., Luan, Y., Yang, X., Jiang, Y., Zhao, L., Zong, Y., and Li, Z. "Functionalized Mesoporous Silica Particles for Application in Drug Delivery System." *Mini Reviews in Medicinal Chemistry* 12.8 (2012): 775-788.

71. Vallet-Regí, M., Balas, F., and Arcos, D. "Mesoporous materials for drug delivery." *Angewandte Chemie International Edition* 46.40 (2007): 7548-7558.

72. Vallet-Regi, M., Ramila, A., Del Real, R. P., and Pérez-Pariente, J. "A new property of MCM-41: drug delivery system." *Chemistry of Materials* 13.2 (2001): 308-311.

73. Horcajada, P., Ramila, A., Perez-Pariente, J., and Vallet-Regı, M. "Influence of pore size of MCM-41 matrices on drug delivery rate." *Microporous and Mesoporous Materials* 68.1 (2004): 105-109.

74. Gomez-Vega, J. M., Sugimura, H., Takai, O., and Hozumi, A. "Aligned bioactive mesoporous silica coatings for implants." *Journal of Materials Science: Materials in Medicine* 12.10-12 (2001): 923-927.

75. Gomez-Vega, J. M., Hozumi, A., Saiz, E., Tomsia, A. P., Sugimura, H., and Takai, O. "Bioactive glass–mesoporous silica coatings on Ti6Al4V through enameling and triblock-copolymer-templated sol-gel processing." *Journal of biomedical materials research* 56.3 (2001): 382-389.

76. Wang, X., Li, X., Onuma, K., Ito, A., Sogo, Y., Kosuge, K., and Oyane, A. "Mesoporous bioactive glass coatings on stainless steel for enhanced cell activity, cytoskeletal organization and AsMg immobilization." *Journal of Materials Chemistry* 20.31 (2010): 6437-6445.

77. Xia, W., Grandfield, K., Hoess, A., Ballo, A., Cai, Y., and Engqvist, H. "Mesoporous titanium dioxide coating for metallic implants." *Journal of Biomedical Materials Research Part B: Applied Biomaterials* 100.1 (2012): 82-93.

78. Ehlert, N., Badar, M., Christel, A., Lohmeier, S. J., Luessenhop, T., Stieve, M., Lenarz, T., Peter, P. M., and Behrens, P. "Mesoporous silica coatings for controlled release of the antibiotic ciprofloxacin from implants." *Journal of Materials Chemistry* 21.3 (2011): 752-760.

79. Shimura, Naoki, and Makoto Ogawa. "Deposition of thin mesoporous silica films on glass substrates from basic solution." *Journal of colloid and interface science* 303.1 (2006): 250-255.

80. "FT-IR Spectroscopy Attenuated Total Reflectance (ATR)." *Technical Note. PerkinElmer Life and Analytical Sciences.*

81. Pierotti, R. A., and Rouquerol, J. "Reporting physisorption data for gas/solid systems with special reference to the determination of surface area and porosity." *Pure and Applied Chemistry* 57.4 (1985): 603-619.

82. Sattler, K. D. "Nanoporous materials." *Handbook of Nanophysics: Functional Nanomaterials.* Boca Raton: CRC Press (2011): 9-7.

Curriculum Vitae

Name:	Afrah Al Hegy
Post-secondary Education and Degrees:	King Faisal University Alhassa, Saudi Arabia 2003-2007 B.Sc. Chemical Education
	Laurentian University Sudbury, Ontario, Canada 2012-2014 M.Sc. Chemical Sciences (in progress)
Honours and Awards:	**Graduate Studies Scholarship**
	Ministry of Higher Education in the Kingdom of Saudi Arabia.

Conference Presentations:

1. **A. Alhegy**, J. E. Gray-Munro "Deposition of a Mesoporous Silica Coating on Magnesium Alloy AZ31" presented at the Materials Science and Technology Conference, Montreal, QC, October 2013 (Oral Presentation)

2. **A. Alhegy**, J. E. Gray-Munro "Deposition of a Mesoporous Silica Coating on Magnesium Alloy AZ31" presented at the International Conference on Nanotechnology and Advanced Materials, Quebec, PQ, August 2013 (Poster)

3. **A. Alhegy**, J. E. Gray-Munro "Deposition of a Mesoporous Silica Coating on Magnesium Alloy AZ31" presented at the Canadian Biomaterials Society Conference, Ottawa, ON, May 2013 (Poster)